



Development of a measurement system for wafer-level measurements

Master Thesis

Rick Buijvoets (4936663)

Development of a measurement system for wafer-level measurements

by

Rick Buijvoets (4936663)

Supervisor (Flexous): Gerard Dunning
Supervisor (TU Delft): Jens Kober
Project Duration: February, 2024 - May, 2025



Summary

This report presents a comprehensive evaluation of a measurement system for measuring the frequencies of Flexous oscillators while they are still in the wafer integrated with the Prusa I3 MK3 3D printer. The study focusses on assessing the precision, repeatability, and edge detection capabilities of the system through a series of meticulously designed experiments. The findings provide valuable insights into the performance of the integrated 3D printing mechanics and sensor feedback under conditions demanding high precision.

The final design of the automated testing setup intended for precise laser-based frequency measurements of oscillators is shown in Chapter 3. The design is centred on a lead screw-driven positioning system, selected for its accuracy, repeatability, and mechanical reliability. The mechanical frame is constructed from aluminium extrusion profiles offering rigidity and modularity, while stepper motors, coupled via flexible couplings to lead screws, enable controlled motion in the x- and y-directions. Linear bearings and guide rails ensure smooth and constrained movement of the laser assembly.

The key factors affecting positional accuracy are addressed, including microstepping, backlash, and structural deflection. Microstepping enhances movement smoothness and resolution by subdividing each motor step, though it has limited impact on absolute positioning due to mechanical nonlinearities. Backlash, a major source of inaccuracy, is mitigated using anti-backlash nuts, which apply continuous pressure to eliminate play between the nut and screw, improving repeatability and reducing mechanical wear.

Deflection analysis is performed to assess how load-induced deformation and material elasticity may impact the accuracy of measurement. Using free-body diagrams and beam theory, it is demonstrated that the maximum deflection of the system is less than $10\mu\text{m}$, which is well within the laser measurement range 0.3 mm . The angle deviation from the deflection is on the order of 10^{-5} degrees, confirming that structural flexibility does not compromise laser alignment.

The calibration procedure involves moving the laser toward the oscillator until it precisely aligns with the boundary, ensuring consistent measurement initiation. The setup incorporates the Micro-Epsilon IFS2405 laser, already validated in manual procedures.

Finally, an activation mechanism is included to initiate oscillator vibrations. This uses a speaker-generated sound pulse, channelled through tubing to create an airflow that excites the oscillator. The overall system is modular, robust, and designed for future scalability, enabling reliable and accurate automated frequency measurements.

The homing accuracy tests were conducted to determine the printer's ability to consistently return to its predefined home position, a critical factor for ensuring reliable and repeatable measurement results. The results demonstrated substantial positional consistency, with deviations predominantly within the micrometre range. In particular, the Y-axis exhibited superior repeatability compared to the X-axis, as evidenced by a reduced interquartile range and fewer outliers in the boxplot analysis. This suggests that the movements on the Y-axis are more consistent, whereas the X-axis shows greater variability, potentially due to mechanical influences such as belt tension or stepper motor performance.

Despite these disparities, the generally minimal deviation observed across both axes indicates that the homing function possesses sufficient robustness for reliable initialisation. However, the greater spread and occurrence of outliers within the X-axis data imply possible mechanical influences that warrant further investigation. Enhancing the consistency of endstop engagement or refining the behaviour of the printer firmware during the homing process could contribute to reducing the frequency of outliers and lead to a narrower deviation range.

Movement accuracy tests were designed to assess the precision with which the system could reach specified positions from a predetermined reference point. The Mean Absolute Error analysis over different distances revealed that the Y-axis persistently exhibited higher errors compared to the X-axis. This could be partially attributed to sensor alignment issues or mechanical characteristics of the movement system. Additionally, the measurement block used for the Y-axis test might have contributed to increased uncertainty.

The absence of a direct correlation between travel distance and absolute error suggests that the inaccuracies may not be only systematic. Instead, a combination of random error sources, such as micro-stepping inconsistencies in the stepper motor, elasticity of the belt or thermal expansion, along with minor misalignments, are likely contributing factors.

Future research could explore the implementation of real-time feedback correction or closed-loop control systems, where positional data obtained from external sensors may be used to dynamically adjust the final positioning of the toolhead. Such enhancements could mitigate observed inaccuracies and improve overall movement precision.

The system's ability to consistently return to an identical position following multiple movements is essential for maintaining consistent measurement results. Repeatability tests indicated significant consistency, with the Y-axis again demonstrating superior performance, as evidenced by a narrower distribution and reduced scatter in the normal curve plot. Despite a persistent offset between the actual returned position and the intended target.

Such systematic biases are frequently observed in open-loop systems, similar to those used in many 3D printers, where the accuracy of movements is presumed unless explicitly corrected. The predictable nature of this deviation offers an opportunity for rectification through hardware-based compensation. By incorporating a closed-loop feedback mechanism, it would be feasible to identify and actively correct any positional discrepancies as they arise, thereby enhancing the system's repeatability and overall accuracy.

Accurate calibration and edge detection are critical for ensuring that the laser aligns precisely with the intended targets, thereby guaranteeing reliable measurement. The findings of the edge detection tests demonstrated a distinct and consistent offset between the detected edge and the actual edge, with an average deviation of approximately 0.6 mm. This discrepancy was mainly attributed to the default speed settings in the calibration script.

To further explore this issue, subsequent tests evaluated the impact of varying the calibration speeds on detection accuracy. As hypothesised, lower speeds resulted in markedly reduced errors, with measurements at 10 and 20 mm/min producing mean absolute errors of less than 0.05 mm. In contrast, as the speeds increased, the positional error also increased significantly, with values rising substantially above 40 mm/min. These results suggest a direct trade-off between operational speed and edge detection fidelity.

The observed error is attributable to a combination of physical factors, including the momentum of the system and the finite update rate of the sensor, as well as software constraints, such as the rate at which sensor readings are analysed and acted upon. At elevated velocities, the system's inability to decelerate promptly upon edge detection results in overshoot, compromising the precision of the calibration process.

Implementing predictive stopping logic could enhance the system's performance by anticipating the detection point and allowing for smoother transitions and proactive adjustments. This approach takes advantage of real-time data to improve efficiency, reduce reaction times, and minimise errors. By analysing velocity, deceleration, and other relevant parameters, the system can predict the optimal stopping point with greater accuracy, thus improving overall calibration precision.

Contents

Summary	i
1 Introduction	1
2 Background	3
2.1 Stakeholders	3
2.1.1 Stakeholder Identification	3
2.1.2 Stakeholder Interests and Influence	4
2.2 Accuracy vs. Precision	4
2.3 Goal	5
2.4 Requirements	5
3 Design	8
3.1 Concepts	8
3.1.1 Linear Stages	8
3.1.2 XY-stages	9
3.1.3 CoreXY System	9
3.1.4 Lead Screw	10
3.1.5 Concept comparison	11
3.2 Final Design	12
3.2.1 Positioning	12
3.2.2 Calibrating	16
3.2.3 Activation of vibration	17
3.2.4 Complete Design	17
4 Testing & Results	19
4.1 Testing	19
4.1.1 Changes	19
4.1.2 Setup	19
4.1.3 Plan	20
4.2 Results	22
4.2.1 Verify Initial Position	22
4.2.2 Accuracy of X and Y axis	23
4.2.3 Repeatability of X and Y axis	23
4.2.4 Edge Detection Accuracy	24
4.2.5 Edge Detection Speed	25
4.3 Overall result	25
5 Discussion & Conclusion	26
5.1 Homing accuracy	26
5.2 Movement Accuracy	26
5.3 Repeatability	26
5.4 Calibration & Edge Detection	27
5.5 Future Work	27
References	28
A Deflection Calculation	29
B Code	33
B.1 Code for Movement	33
B.2 Code for Calibration	34

1

Introduction

In the semiconductor industry, wafer-level measurements ensure quality, reliability, and performance. As device dimensions continue to shrink and complexities increase, the accuracy and precision of these measurements become more critical. A wafer, being a thin slice of semiconductor material, usually silicon, is the foundational substrate on which devices are fabricated. The fabrication process involves multiple steps, including photolithography, etching, doping, and deposition, all of which require stringent control and monitoring to achieve the desired characteristics [1]. To meet the ever-increasing demand for high-performance, it is imperative to develop sophisticated measurement systems that can provide detailed insights into the characteristics of the devices on the wafer.

The existing measurement techniques for wafer-level testing are often constrained by factors such as limited resolution, inadequate throughput, and susceptibility to environmental variations. As the industry progresses towards more advanced technologies, the limitations of traditional measurement systems become more pronounced, necessitating the development of new methodologies and tools. The drive for innovation in this field is further driven by the need to reduce manufacturing costs, improve yield rates, and accelerate the time to market for new technologies.

The interest of the industry lies in its potential to fundamentally improve the way frequency measurements are conducted for semiconductor products. Unlike conventional methods that require devices to be separated from the wafer for testing, which introduces handling risks, delays, and added costs, this project proposes a wafer-level solution. The ability to perform precise, contactless frequency measurements on intact wafers is not only innovative, but also aligns with the industry's trend toward greater automation, miniaturisation, and throughput. By bridging the gaps between metrology, system engineering, and semiconductor manufacturing, the proposed approach offers a novel solution that addresses both technical and economic challenges in modern device fabrication.

Flexous is a Dutch company that specialises in high-performance oscillators for mechanical watches, revolutionising the precision of timekeeping mechanisms. Oscillators are essential components in mechanical watches that determine the accuracy of timekeeping. This master thesis focusses on developing a testing setup capable of measuring the frequency of Flexous oscillators. Accurate frequency measurement is crucial for quality control, product development, and optimising performance.

The main objective of this research is to develop a robust and accurate measurement system tailored explicitly for the frequency characterisation of Flexous oscillators while they are still in the wafer stage of production. The measurement of frequency at this stage presents unique challenges, including the need for high accuracy and the ability to handle many oscillators. Traditional frequency measurement methods often require the separation of individual devices from the wafer, a process that can introduce errors and reduce throughput. By enabling wafer-level measurements, this system aims to enhance the accuracy, efficiency, and scalability of the testing process.

The primary objective of the research presented in this Master's Thesis is to design, develop, and validate an advanced measurement system specifically designed for the oscillators of Flexous. This system is able to position, measure, and characterise the oscillators while they remain on the wafer. The research adopts a multidisciplinary approach that combines engineering and metrology principles

to tackle the challenges of wafer-level assessments. This work aims to advance knowledge in the following key areas:

1. **Design and Development:** To design a wafer-level measurement system that integrates state-of-the-art sensors, data acquisition hardware, and software algorithms capable of performing high-resolution measurements with minimal uncertainty.
2. **System Validation:** To validate the performance of the developed system through experimental tests on actual semiconductor wafers, comparing the results with those obtained from conventional measurement systems.
3. **Cost-Effectiveness:** To evaluate the cost-effectiveness of the developed system compared to existing solutions, taking into account factors such as material costs, operational efficiency and potential savings from reduced defect rates.

These objectives culminate in the following research question for this Master Thesis:

How can a high-precision measurement system be developed and optimised to accurately measure the frequency of Flexous oscillators while still on the wafer?

The development of a measurement system for wafer-level measurements has significant implications for Flexous. As the demand for producing more oscillators continues to increase, the ability to precisely measure and control the fabrication process at the wafer level becomes increasingly important. The proposed system is expected to contribute to the advancement of Flexous's operations. By fulfilling the defined objectives, this thesis establishes a solid foundation for future research efforts aimed at developing an advanced measurement system. Such a system has the potential to significantly enhance the accuracy and efficiency of frequency measurements for flexible oscillators while remaining on the wafer. Consequently, Chapter 2 presents the contextual background, including an overview of key stakeholders and the derivation of the system requirements. Chapter 3 details the conceptual development process, including an evaluation of multiple design alternatives leading to the selection of the final design. The experimental methodology and the corresponding results are presented in Chapter 4. Finally, the findings are critically analysed in the discussion and overarching conclusions are drawn in Chapter 5.

2

Background

2.1. Stakeholders

A detailed stakeholder analysis is essential to identify the parties involved, their interests, and how they may be affected by the development of the testing setup. This process helps ensure effective communication, aligns project goals with stakeholder expectations, minimises resistance, and promotes collaboration throughout the design, calibration, and implementation phases.

2.1.1. Stakeholder Identification

The development of a testing setup to measure the oscillator frequency involves several stakeholders, both internal and external. These groups have varying degrees of interest and influence on the success of the project. Stakeholders can be classified into internal and external categories.

Internal Stakeholders:

- **Founders and Executive Team:** The executive team is responsible for the overall direction, research priorities, and market strategy of the company. Their interests align with improving product quality and ensuring that the company maintains a competitive edge. A testing setup that improves oscillator performance would benefit Flexous's product offerings and market reputation.
- **Engineers and R&D Team:** This group is at the core of Flexous's innovation, developing and refining oscillator designs. The testing setup directly impacts them as it will enhance their ability to measure, validate, and optimise oscillator performance.
- **Production Team:** Once a product is in production, consistent and precise testing is required to ensure quality across all units. The production team will use the developed testing setup for routine quality checks, making their interest in the project focused on ease of use, accuracy, and efficiency.

External Stakeholders:

- **Watch Manufacturers (Clients):** Mechanical watch manufacturers who would integrate Flexous's oscillators into their timepieces are crucial external stakeholders. Their interests lie in the reliability and precision of Flexous's products, which directly impact the performance of their watches. A robust testing setup ensures that only oscillators that meet the highest standards are delivered to them.
- **Regulatory Institutions and Industry Standards Organisations:** The watchmaking industry operates under strict guidelines, especially in terms of accuracy and performance. Regulatory bodies ensure that watches meet specific precision standards. The testing setup must align with these standards to ensure compliance, making regulatory bodies critical stakeholders.
- **Competitors:** Other companies specialising in oscillator technology will closely monitor Flexous's advances. A successful testing setup that improves product performance could influence the competitive landscape. Competitors may seek to replicate or counter Flexous's advancements.
- **Watch Collectors and Enthusiasts:** Although not direct customers of Flexous, watch collectors and enthusiasts are often vocal influencers in the market. They are deeply interested in technological innovations that improve watch performance.

2.1.2. Stakeholder Interests and Influence

The Founders and Executive Team of Flexous are focused primarily on driving business growth, securing market leadership, and fostering technical innovation. Their goal is to ensure that Flexous remains competitive in the precision watch market. They are highly influential in this process, as they make key decisions regarding strategic investments in research and development, including the approval of resources necessary for the development of the new testing setup for oscillators.

The Engineers and R&D Team have a vested interest in the technical accuracy of the products they develop and in continually refining the performance of the oscillators. This team will benefit the most from a testing setup that provides real-time, precise measurements of the oscillator frequency, as it will directly influence their ability to innovate and improve the technology. Their influence is high, given that they will contribute and shape both the development of the setup.

The Production Team is concerned with the ease of use, scalability, and seamless integration of the testing setup into the manufacturing process. Their primary interest lies in ensuring that the setup is efficient and minimises disruption to their workflow while ensuring consistent production output. Their influence is medium, as it must meet their operational needs to be successfully implemented.

Watch manufacturers (clients) who ultimately use Flexous oscillators in their timepieces are very interested in reliable, high-performance oscillators that improve both the accuracy and prestige of their watches. Their influence is high, as their satisfaction directly impacts Flexous's reputation and success. Regulatory bodies focus on ensuring compliance with industry standards for accuracy and performance. They require the testing setup to align with specific metrics. Their influence is medium to high, as regulatory compliance is necessary for product certification, especially in the luxury mechanical watch market.

Competitors are interested in keeping track of Flexous's technological advancements. They aim to benchmark these innovations to match or exceed them. Although their influence is low to medium, a successful testing setup could alter competitive positioning and market dynamics.

Finally, Watch Collectors and Enthusiasts are interested in precision, innovation, and craftsmanship in mechanical watches. They are always on the lookout for watches that push technological boundaries. Although they may not be direct buyers of Flexous's oscillators, their opinions and preferences can influence the broader market demand. Their influence is medium, as they can indirectly impact the desirability of products featuring Flexous oscillators.

Developing a test setup to measure the frequency of Flexous oscillators involves multiple stakeholders with varying interests and degrees of influence. By understanding these stakeholders and aligning the project goals with their needs, the master thesis can ensure that the testing setup is technically robust and aligned with market and regulatory demands. This alignment will improve Flexous's position as a leader in the high performance oscillator market and strengthen its relationships with clients, investors, and industry partners.

2.2. Accuracy vs. Precision

During this project, the terms accuracy and precision will be used frequently. Those terms are frequently mixed up, so this section will explain the definitions of the terms accuracy, precision, and resolution.

Accuracy

Accuracy is the measure of how close a result is to the true or correct value [2]. It is commonly used to assess the reliability of measurements, predictions, or classifications. High accuracy means fewer errors, while low accuracy indicates significant deviations from the correct value. Accuracy differs from precision; while precision focusses on consistency, accuracy emphasises correctness.

Precision

Precision, also called repeatability, refers to the consistency and repeatability of measurements. It indicates how closely multiple results align with each other, regardless of their accuracy [2]. Figure 2.1 show a summary of the definitions of accuracy and precision.

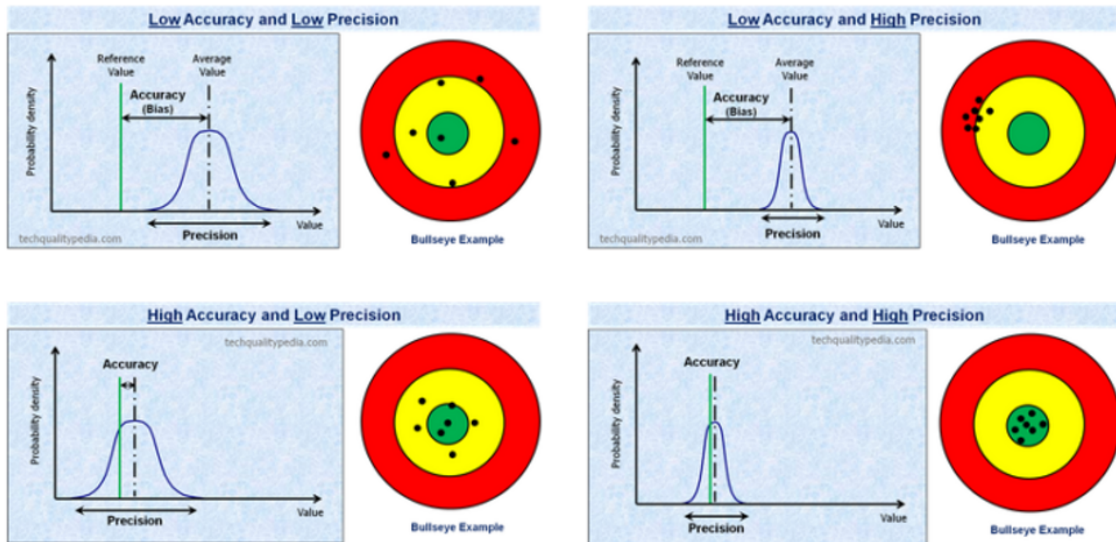
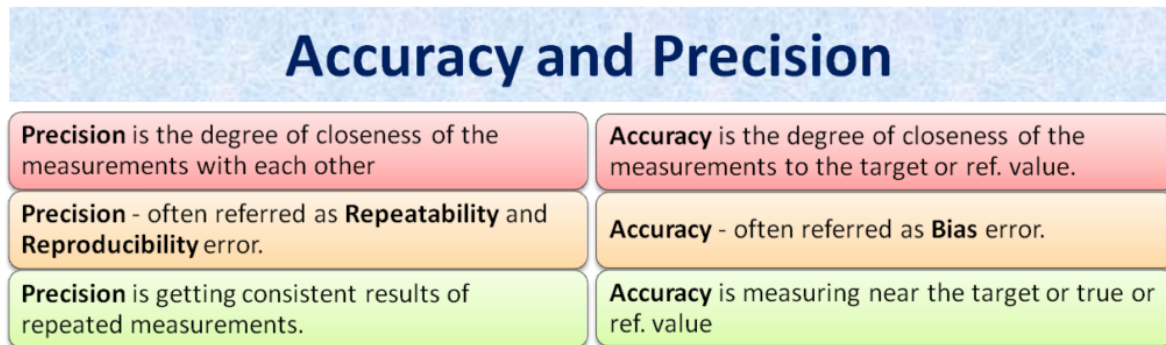


Figure 2.1: Summary of accuracy vs precision [3]

Resolution

Minimum incremental motion (MIM) refers to the smallest movement that a device can consistently and reliably achieve. It is also known as practical or typical resolution. MIM is influenced by both mechanical and electrical components, including the drive mechanism (such as a screw), guide system, motor, controller, and encoder. Due to the complexity of these factors and the difficulty of accurately modeling friction, MIM is determined through empirical testing rather than theoretical calculations.

2.3. Goal

An oscillator, as shown in Figure 2.2, has a diameter of approximately 10 millimetres. To measure its frequency, a laser will be aligned with the edge of the oscillator. As the oscillator vibrates, the laser can detect its frequency. Currently, Flexous performs this frequency measurement manually. The goal of the new testing setup is to reduce both the cost and the time associated with this process. The system should be capable of measuring the frequency while the oscillators remain in the wafer. Each wafer contains 55 oscillators, as illustrated in Figure 2.3. Given the small size of the components, the system must provide high accuracy and precision. Therefore, the objective of this project is to design and evaluate a high-precision testing setup that can measure oscillator frequencies directly on the wafer. With the goal clearly defined, the corresponding requirements can now be established. These are outlined in the next section.

2.4. Requirements

Certain requirements have been established to prioritise this project, using the MoSCoW method [4]. This approach categorises requirements into must-haves, should-haves, and could-haves, where each

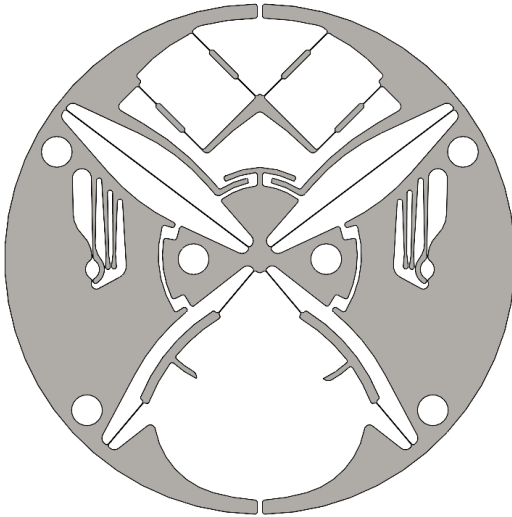


Figure 2.2: An oscillator from Flexous

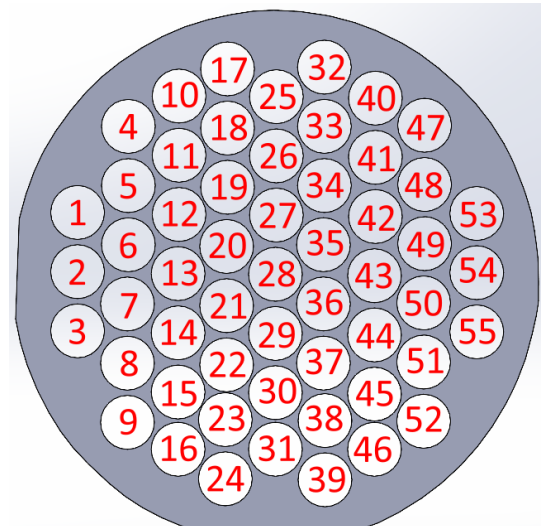


Figure 2.3: An wafer with 55 places for an oscillator

term is defined as follows:

- Must have** - requirements that the system must have. Otherwise, the system will not function.
- Should have** - requirements that the system should have, but it will function well without these requirements.
- Could have** - requirements that the system could have, but only when time is left to implement these requirements.

Must Haves

1. The setup must be able to measure the frequency of 55 oscillators in one wafer in one running cycle.
2. The actuators must be able to position the oscillators with an accuracy of 10 microns.
3. The setup must be able to initiate vibrations of the oscillators.
4. The measured frequency must be automatically logged to save the data.
5. The setup must be robust to handle continuous testing without performing loss.
6. The setup must have a control system that controls the adjustments of the axes.
7. The system must include an automatic calibration feature to maintain the accuracy of the measurements over time.
8. The system must be capable of performing measurements rapidly to handle high-volume testing requirements.
9. To prevent measurement errors, the setup must be designed to minimise and isolate external vibrations and electromagnetic interference.
10. The control system must be capable of making real-time adjustments based on feedback from the measurements.

Should Haves

1. The setup should have a bed where the wafer can be easily placed and removed within 10 seconds.
2. The system should have a user-friendly interface, which makes it easy for personnel to operate.
3. Real-time monitoring should be available to check if the setup is still functioning.
4. The device should be able to move to a specific oscillator and measure the oscillator when the operator gives the command.
5. The system should automatically generate reports after each batch of tests, summarising the results and highlighting any issues.

6. The system should automatically detect and flag measurement errors or anomalies for review.
7. The system should log detailed information about each test, including timestamps, environmental conditions, and any anomalies detected.
8. The setup should log errors and operational issues for troubleshooting.

Could Haves

1. The system could support remote access and control for monitoring off-site.
2. The setup could have maintenance alerts and reminders to ensure consistent performance.
3. The device could have self-diagnostic tools for troubleshooting and maintenance.
4. The system could be flexible to accommodate different wafer sizes and configurations.
5. The testing setup could have customisable reporting features for documenting the test results.
6. The system could have advanced visualisation tools for data interpretation.
7. The setup could support batch processing of multiple wafers to improve efficiency.
8. The setup could be designed for energy efficiency to reduce operational costs.
9. The system could have remote access to control and monitoring via a web interface.
10. The system could have an auto shut-off feature to save power.
11. The setup could have safety features to prevent injuries to personnel or damage to equipment.
12. The setup could have a reliable power supply and backup to prevent data loss when the power goes down.
13. The setup could be modular for easy expansion and upgrades when needed.
14. The design could be portable so that testing can be done in different locations in or outside the building.
15. The device could have the ability to integrate existing laboratory equipment.

3

Design

3.1. Concepts

One of the most critical requirements for this project is achieving accurate positioning. Proper positioning is essential to ensure that measurements are carried out properly. To meet this requirement, various approaches and techniques that could improve precision are necessary.

To begin with, several concept designs for movement were created to investigate different possibilities to fulfil the accurate positioning requirement. These concepts served as a way to visualise and experiment with multiple methods, helping to better understand the potential solutions and associated challenges. By prototyping and refining these concepts, it became easier to identify strengths and weaknesses, as well as areas where adjustments were needed to improve accuracy. First, a linear stage is analysed followed by a few XY stages. In addition, the CoreXY system and a system with lead screws are analysed.

3.1.1. Linear Stages

This system uses two linear stages mounted in a stacking configuration, where one stage is placed perpendicularly to the other on top to allow planar movement with two degrees of freedom, as shown in Figure 3.1. Each stage consists of a base, carriage, guide rails, and actuator, which work together to provide precise and independent motion along a single axis. When combined, the setup offers high-precision movement in both directions with micrometre-level accuracy.

A key advantage of this stacked configuration is its compact, space-efficient design, making it well suited for environments with spatial constraints. Independent control of each axis allows for versatile and precise motion, accommodating a broad range of applications and complex movement patterns. However, this approach introduces an increase in the mechanical and control complexity. Coordinating the two stages requires careful synchronisation to avoid misalignment or interference. In addition, the system is susceptible to vibrations and mechanical wear, which can degrade accuracy over time, underscoring the need for routine maintenance and calibration.

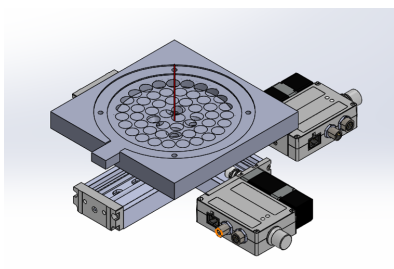


Figure 3.1: Two linear stages on top of each other

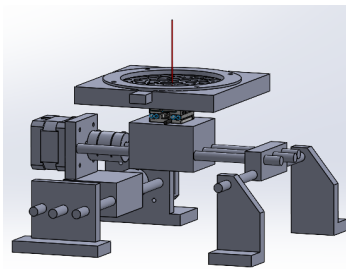


Figure 3.2: Piezoelectric XY stage in combination with stepper motors

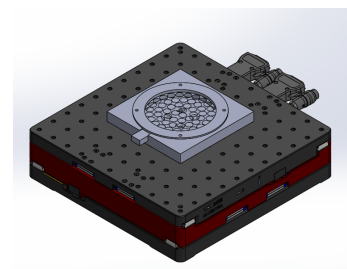


Figure 3.3: High-precision XY-stage with DC motors

3.1.2. XY-stages

This section will explore a few different XY-stages. First, it delves into a piezoelectric XY-stage and after that it continues with a high-precision XY-stage.

Piezoelectric XY-stage

The concept in Figure 3.2 combines coarse and fine motion capabilities by integrating stepper motors with piezoelectric actuators. Coarse positioning is achieved using stepper motors and linear rails, while high-resolution adjustments are performed by piezo actuators, which expand or contract under an applied electric field [5]. This setup allows for both high-speed travel and submicrometer positioning precision.

Piezoelectric actuators offer several advantages, including nanometre-level accuracy, rapid response times, and frictionless motion that eliminates mechanical wear and backlash [6]. This ensures a stable and highly repeatable position.

However, the limited travel range of piezo elements necessitates integration with stepper motors and feedback systems such as encoders. Furthermore, piezoelectric materials can exhibit hysteresis and drift, requiring active compensation techniques to maintain precision. The inclusion of these high-precision components contributes to increased system cost, making such setups more suitable for specialised or high-end applications.

High-precision XY-stage

The high-precision stage system, as shown in Figure 3.3, is engineered to deliver 150mm of travel in both the X and the Y directions, supporting submicrometer positioning accuracy. Driven by brushless DC motors, the motion is precise and low-wear, while high-rigidity linear bearings ensure structural stability and minimise backlash during operation. Integrated optical encoders provide real-time feedback, allowing the system to achieve an on-axis accuracy of $\pm 10\mu\text{m}$ and a bidirectional repeatability of $\pm 0.30\mu\text{m}$ [7], making it highly suitable for demanding precision applications.

The use of brushless motors offers additional advantages, such as increased durability, reduced maintenance requirements, and lower thermal output. However, the system is not without challenges. Over time, mechanical wear, particularly in bearings, can degrade performance, which requires regular maintenance. Moreover, the overall cost of the setup is significant, including both the stage and its associated controller.

3.1.3. CoreXY System

CoreXY is a motion control system widely used in 3D printers, laser cutters, and other precision machinery. Known for its speed, accuracy, and efficient design, CoreXY enables high-performance XY-plane movement with fewer moving parts compared to traditional Cartesian setups. This section discusses the working principle, advantages, and challenges of implementing CoreXY.

Principle

As illustrated in Figure 3.4, CoreXY operates using two stationary motors and a crossed belt system to drive the movement in the XY plane. Unlike Cartesian systems, where each motor drives one axis, CoreXY coordinates both motors to move the toolhead. Rotating the motors in the same direction moves the tool diagonally, while opposite rotations result in linear X or Y movement. This configuration enables smooth, controlled motion with fewer mechanical components in motion.

The cross-belt design and fixed motors reduce the moving mass, which improves overall stability and responsiveness [8]. This also allows for faster acceleration and deceleration, making CoreXY ideal for high-speed applications requiring precision.

Advantages

CoreXY offers several mechanical and operational benefits. The stationary motors reduce vibrations and mechanical wear, while the lightweight moving assembly enhances speed without compromising accuracy. Its compact layout makes it suitable for space-constrained systems, and the simple, planar structure eliminates the need for complex gantries or additional support.

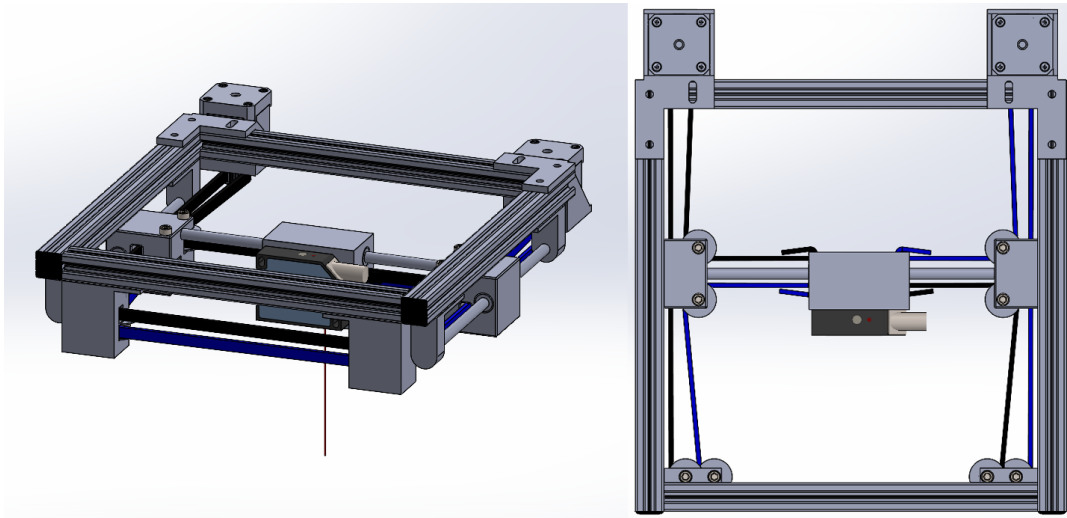


Figure 3.4: CoreXY system. Left complete overview and right top view of the system.

Challenges

Despite its advantages, CoreXY comes with some implementation challenges. The belt system is more complex than in basic Cartesian designs and requires precise assembly and consistent tensioning. Belt stretching, wear, or slippage can introduce errors over time, so regular inspection and maintenance are necessary.

Accurate motion also depends on perfect synchronisation of the two motors. Even slight misalignment can lead to positional errors, which requires high-quality stepper drivers and firmware to maintain consistent performance. In addition, the need for precision components, such as belts, pulleys, and electronics, can increase initial costs compared to simpler setups.

3.1.4. Lead Screw

To achieve high accuracy linear motion in precision applications, screw-driven lead systems offer a reliable and efficient solution. This section explores the construction, functionality, and performance trade-offs of such a setup.

The movement mechanism, as shown in Figure 3.5, is driven by lead screws, offering high accuracy and repeatability of the position. The system employs linear bearings for smooth translational motion along the X and Y axes. The top view clearly shows the arrangement of the two lead screws that control the X and Y axes.

Lead screws provide accurate and backlash minimised movement, ideal for measurement or calibration setups. In addition, the aluminium profile frame ensures minimal deflection and high structural integrity. Components can be easily replaced or reconfigured, enabling flexible experimentation.

Lead screws are slower than belt-driven systems, which could limit cycle times in repetitive tasks. Lubrication and cleanliness are crucial to prevent wear or jamming. Precision components such as lead screws and linear guides add to the overall cost of the system.

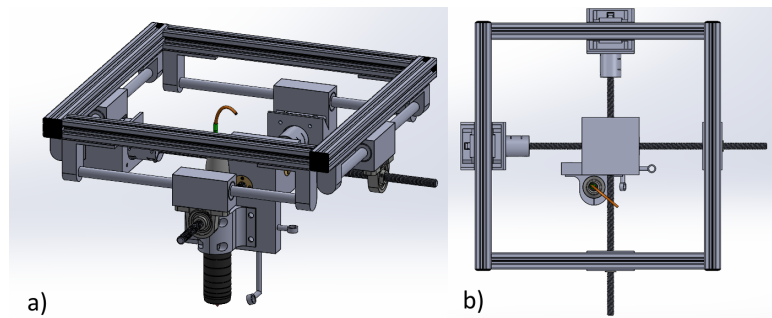


Figure 3.5: A system with lead screws. a) shows a complete overview while b) shows the top view of the system.

3.1.5. Concept comparison

The above sections examine different mechanical designs and techniques to achieve a precise positioning that could be used for the test setup, focussing on precision. This section will compare these concepts and describe the decision-making process for the final design.

The concepts discussed in Section 3.1.1 and Section 3.1.2 may be appealing, offering high accuracy, but their high costs make them less accessible. The concept of the CoreXY principle, discussed in Section 3.1.3, looks feasible with respect to the budget. However, the accuracy of this principle depends on a few factors.

The linear stages and the high-precision XY-stage possess a travel range of 150 mm, which suffices to encompass the entirety of the wafer. In contrast, the piezoelectric XY-stage is characterised by a travel range limited to only a few millimetres. The travel range of the CoreXY system is subject to determination during the design phase, thus allowing potential coverage of the entire wafer.

The high-precision XY-stage is notably straightforward to integrate into the design, requiring merely its incorporation into the system. Conversely, the piezoelectric XY-stage necessitates precise positional information from the system before movement can commence. While linear stages and CoreXY systems are generally straightforward to implement, their integration demands additional procedural steps. Notably, for the CoreXY system, attention must be paid to the tension of the belt.

Accuracy CoreXY

By using stepper motors, timing belts, and pulleys, it is possible to calculate the movement per step of the motor. This calculation assumes a stepper motor with a step angle of 0.9° . The pitch of the timing belt is 2mm and the amount of tooth of the pulley is 20.

$$\text{Steps per revolution} = \frac{\text{full revolution}}{\text{step angle}} = \frac{360}{0.9} = 400 \quad (3.1)$$

$$\text{Circumference pulley} = \text{tooth pulley} * \text{pitch belt} = 20 * 2 = 40\text{mm} \quad (3.2)$$

$$\text{movement per step} = \frac{\text{circumference pulley}}{\text{steps per revolution}} = \frac{40}{400} = 0.1\text{mm per step} \quad (3.3)$$

The accuracy of the CoreXY principle is 0.1mm per step. However, this is in a perfect world without any errors. Sadly, this world does not exist, which means that this accuracy will be slightly higher because of some errors such as motor and pulley tolerances, backlash, and stretch in the belt.

Accuracy Lead Screws

The accuracy of the CoreXY system is too low, since the requirements state that the accuracy must be 10 microns. Section 3.1.1 shows that an accuracy of the micrometre level can be reached using lead screws and stepper motors. The next calculation shows the accuracy of a system that uses a stepper motor with a step angle of 0.9° , and a lead screw with a pitch of 2mm.

$$\text{Steps per revolution} = \frac{\text{full revolution}}{\text{step angle}} = \frac{360}{0.9} = 400 \quad (3.4)$$

$$\text{movement per step} = \frac{\text{pitch lead screw}}{\text{steps per revolution}} = \frac{2}{400} = 0.005\text{mm per step} \quad (3.5)$$

Of course, the accuracy is significantly higher, as in the CoreXY system. Motor tolerance, backlash, and tolerances such as wear play a role. However, the accuracy of the lead screw is much higher than the accuracy of the CoreXY principle.

Summary

Table 3.1 provides a comparative analysis of the five concepts, evaluating them in four parameters: accuracy, travel range, applicability, and costs. The "+" sign indicates a positive influence of the parameter on the design, signifying that it contributes favourably to achieving the desired results. Conversely, the "-" sign denotes a negative influence of the parameter, implying that it detracts from or hinders the attainment of optimal design performance.

This comparative analysis highlights the trade-offs between accuracy, travel range, applicability, and costs for different motion systems. Although piezoelectric and high-precision XY-stages offer superior accuracy, their high cost and limited travel range restrict their utility to this project. In contrast, linear stages and lead screws provide broader applicability. Although CoreXY systems present a potentially viable option, their accuracy remains insufficient for the specified requirements.

	Accuracy	Travel range	Applicability	Costs
Linear stages	+	+	+	-
Piezoelectric XY-stage	++	-	-	--
High-precision XY-stage	++	+	++	--
CoreXY	+ -	++	+ -	+
Lead Screws	++	++	+	+

Table 3.1: Concepts comparison on different aspects. ++ = very good, + = good, + - = neutral, - = bad, - - = very bad.

The table serves as a useful reference for selecting the appropriate motion system based on specific parameters. The table shows that the lead screw is the most viable option. Therefore, the final design will be designed while lead screws are used for the motion transitioning.

3.2. Final Design

Now that the choice for the moving mechanism has been finalised, the next step is to design the entire testing setup, ensuring that all components work seamlessly together. This includes considering factors such as structural stability, alignment precision, and ease of assembly. The design must accommodate the selected moving mechanism while also meeting the project's specific requirements, as mentioned in Section 2.4.

3.2.1. Positioning

As concluded in the previous section, the positioning mechanism will consist of lead screws. As frequently mentioned previously, this mechanism should be able to position a laser very accurately. Consequently, this section examines the variables that can affect positional accuracy.

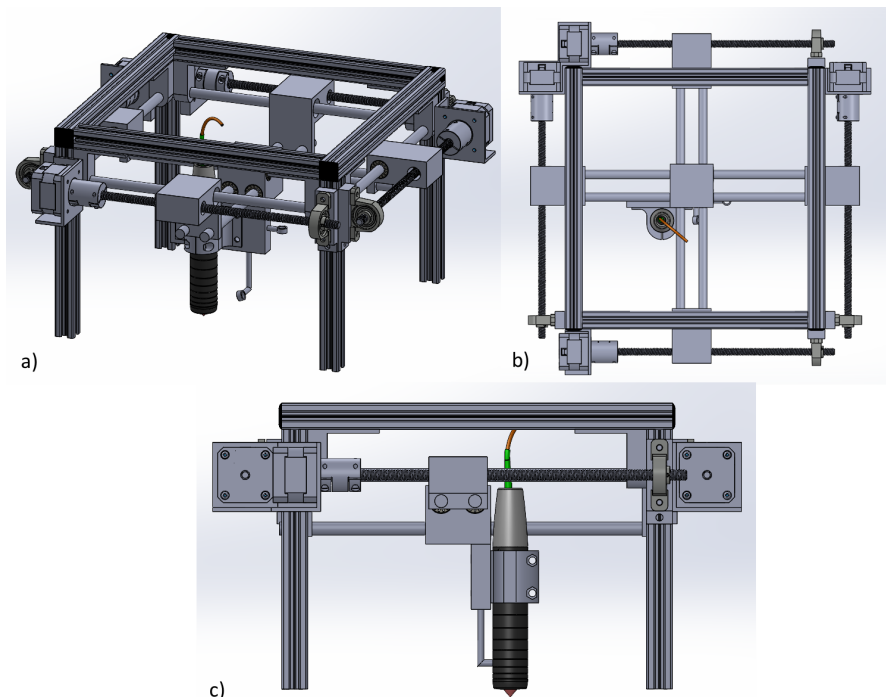


Figure 3.6: Moving mechanism for the setup. a) complete overview, b) top view, c) side view

Design

The final design is shown in Figure 3.6. The frame of the moving mechanism is constructed from extrusion profiles, which confer rigidity and facilitate easy use. Four stepper motors are attached to the frame at three of its corners through specially designed motor brackets. A flexible motor coupling is used to connect the lead screw to the stepper motor. The end of the lead screw is anchored by a bearing to ensure its horizontal alignment and its rotation. A motor is responsible for driving a guiding block by connecting an anti-backlash nut to this block. A linear bearing is incorporated into the block to ensure linear movement along a sliding rod. To move the mass linearly, the motors positioned opposite each other must rotate at identical speeds.

The laser is attached to an intermediary block that moves along linear rods, which are, in turn, connected to the guiding block. This arrangement is designed to facilitate movement in both the x and y directions, necessitating the placement of the rods at varying heights.

The rest of this section will discuss the most important design aspects, such as microstepping, antibacklash nut, and design deformation.

Microstepping

In Section 3.1.5 the resolution of the stepper motor is calculated. However, this calculation did not take into account that stepper motors can have microstepping. Microstepping is a method of driving stepper motors with greater precision by dividing each full step into multiple smaller steps [9]. In traditional stepper motor operation, the rotor moves in discrete angular increments, or full steps, as determined by the motor's step angle. Microstepping achieves finer motion control by modulating the current supplied to the motor's windings using a sinusoidal or approximated waveform.

In standard operation, the motor's windings are energised sequentially with a maximum or zero current, causing the rotor to align with the resultant magnetic field. However, in microstepping, the current in each winding is continuously varied in small increments, as shown Figure 3.7. This creates an intermediate magnetic field, resulting in smoother and smaller rotor movements. For example, dividing a full step into 16 microsteps increases the motor's resolution by a factor of 16.

Microstepping reduces mechanical vibrations and resonance effects, enhancing the motor's performance in precision applications such as robotics, CNC machines, and 3D printers. However, it is important to note that microstepping does not significantly increase the motor's positional accuracy, as the system's mechanical limitations and stepper motor design introduce non-linearities. Basically, it improves smoothness and resolution, making it a valuable technique for applications that require high precision and low noise.

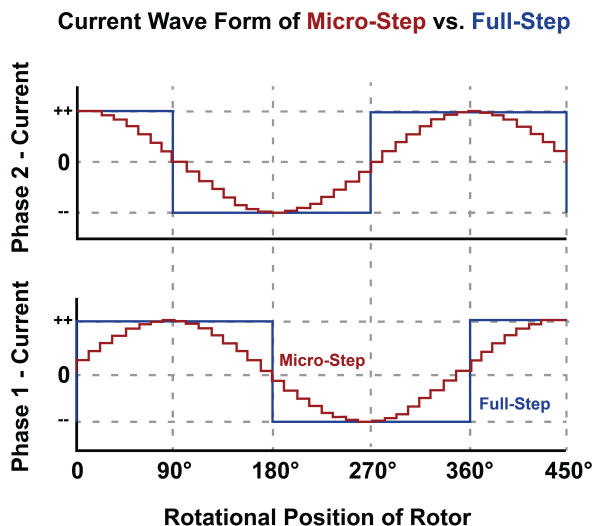


Figure 3.7: Microstepping vs full step [10]



Figure 3.8: Anti-backlash nut [11]

Anti-Backlash Nut

In modern automated systems, precision and repeatability are paramount to successful operation. Whether in CNC machines, 3D printers, or robotic platforms, any deviation in movement can lead

to significant errors in the final output. A common source of inaccuracy in such systems is backlash, which arises from the inherent gap between the lead screw and the threads of the nut. This gap introduces delays when the motion is reversed, leading to positioning errors and mechanical inefficiencies. To address this issue, anti-backlash nuts have been developed to ensure continuous engagement with the lead screw, thereby eliminating unwanted play and improving system performance.

Backlash occurs when a mechanical system exhibits unintended movement due to a clearance gap between interacting components. In lead screw-driven mechanisms, this phenomenon is particularly problematic as it causes discrepancies between commanded and actual positions. The consequences of backlash include reduced precision, poor repeatability, increased wear on mechanical parts, and instability in high-speed applications. Addressing backlash is essential for ensuring smooth and accurate motion, particularly in applications demanding high precision.

An anti-backlash nut, as shown in Figure 3.8, is specifically designed to eliminate unwanted play between the nut and the lead screw. Typically, it comprises a split nut or spring-loaded mechanism that applies continuous pressure on the lead screw threads [12]. This pressure compensates for any gaps, maintaining a consistent mechanical connection. The result is a significant improvement in the accuracy and stability of the system.

Positional accuracy is a critical requirement in automated systems where components must follow exact paths. Standard lead screw assemblies with conventional nuts suffer from backlash-induced deviations, leading to positioning errors. The introduction of anti-backlash nuts eliminates these discrepancies by ensuring that movement commands directly translate into actual motion. As a result, moving systems experience more precise and consistent outcomes.

Repeatability is essential in manufacturing and automation, where a system must return to the same position consistently. Backlash can introduce variability, leading to inconsistencies in product quality or assembly processes. By maintaining a constant mechanical connection, anti-backlash nuts enhance repeatability, ensuring that movements remain identical across multiple cycles. This improvement is particularly beneficial in robotic systems and automated inspection platforms.

Repeated movement with backlash can cause an increase in stress on mechanical components, including lead screws, bearings, and stepper motors. The sudden engagement of slack during directional changes results in impact forces that accelerate wear. Anti-backlash nuts mitigate this issue by maintaining a continuous preload, reducing the likelihood of sudden mechanical shocks. This, in turn, extends the lifespan of the system components and reduces maintenance costs.

Incorporating anti-backlash nuts in lead screw-driven motion systems represents a substantial improvement in precision, repeatability, and mechanical longevity. By eliminating unwanted play, these components ensure that movement commands are accurately translated into physical motion, thus enhancing overall system performance. As automation and robotics continue to advance, the adoption of backlash-free motion solutions will remain a crucial factor in achieving superior operational efficiency and reliability.

Deflection

Deflection in moving systems significantly influences measurement accuracy in scientific and industrial applications. This section examines the causes of deflection, including structural bending, load-induced deformation, and material properties. The effects of these deflections on the measurement are analysed.

One of the primary causes of deflection in this moving system is load-induced deformation. When a force is applied to the structure, the mechanical components experience stress, leading to bending and misalignment. The degree of deflection depends on factors such as the stiffness of the support frame, the weight of the load being moved, and the properties of the lead screws and guide rails. If these components are not sufficiently rigid, they may bend under pressure, causing positional inaccuracies. Lead screws, particularly those of significant length, can deform under tension or compression, further contributing to measurement errors.

Structural bending is another significant factor that affects the precision of measurement. The elasticity of the materials used in the system determines their resistance to bending. A material with a lower Young's modulus will deform more easily under stress, leading to greater deflection. The geometry of the structural components also plays a crucial role; thinner or narrower elements tend to flex more easily than robust, well-supported designs. Furthermore, weak connections between joints can increase the overall deflection of the system, making precise movement difficult to achieve.

By analysing the relationship between applied loads, material properties, and structural geometry, the degree of deflection and its contribution to measurement errors can be determined. Figure 3.9 shows an exaggerated situation when an axis deflects under load. Appendix A shows the full calculation of the deflection.



Figure 3.9: Exaggerated situation of deflection of the axis

Figure 3.10 shows the Free Body Diagram (FBD) of an axis. Because the mass can slide along the axis, a and b are variables. In addition, the force (F) is applied at point C, and the moments (M) and reaction forces (R) of points A and B are also shown.

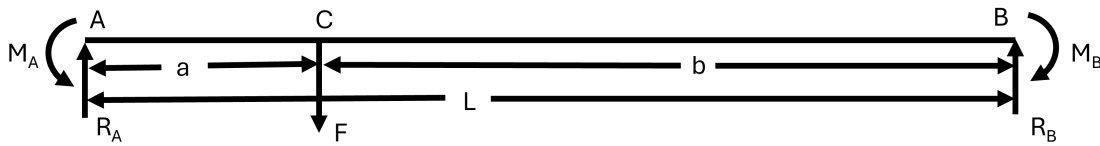


Figure 3.10: FBD of the axis

In Equation (A.1) to Equation (A.6) from Appendix A, the reaction forces and moments are calculated. As a result, the reaction forces are $R_A = \frac{Fb^2}{L^2}(3a + b)$, $R_B = \frac{Fa^2}{L^2}(a + 3b)$, $M_A = \frac{Fab^2}{L^2}$, and $M_B = \frac{Fa^2b}{L^2}$. Given these reaction forces, the angular displacement and deflection formulas can be derived. This derivation is performed in Equation (A.7) to Equation (A.13). In conclusion, the angular displacement and deflection at point C are derived from Equation (A.14) and are illustrated in Equation (3.6) and Equation (3.7), respectively.

$$\theta_C = -\frac{Fa^2b^2}{2EIL^3}(b - a) \tag{3.6}$$

$$y_C = -\frac{Fa^3b^3}{3EIL^3} \tag{3.7}$$

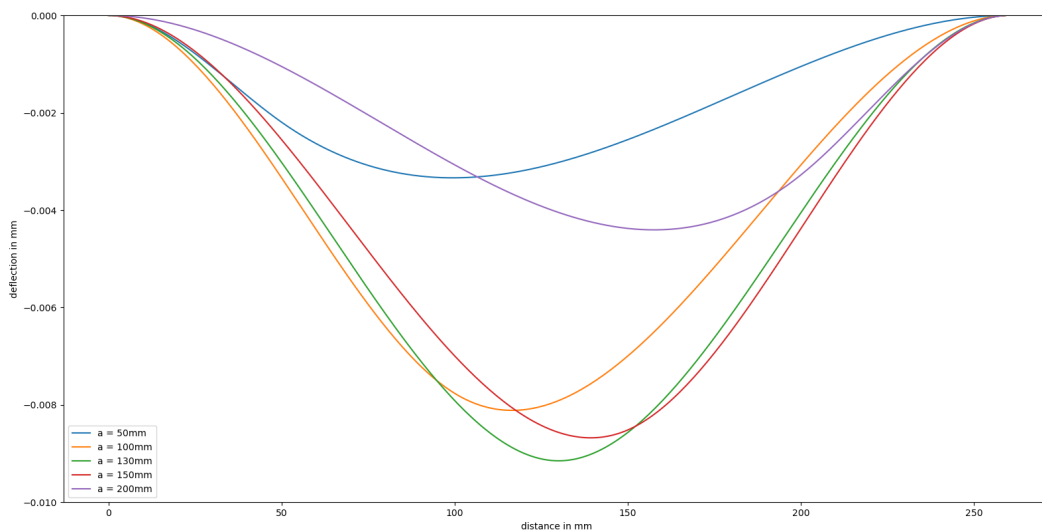


Figure 3.11: The deflection of the guiding rails depending on the position of the mass.

Using the equations described in Equation (A.9) and Equation (A.13), one can generate, as illustrated in Figure 3.11, a plot that depicts the deflection at various positions of the mass. This analysis reveals that maximum deflection occurs when the mass is centrally positioned within the axis. Examination of the plot indicates a negligible impact on positional accuracy, as deflection is gradual and does not induce substantial tilting or angular deviations. As illustrated in Figure 3.12, deflection may result in misalignment of the laser with respect to the oscillator. However, the calculation of this angle indicates that it will be approximately on the order of 10^{-5} degrees. Consequently, this factor will not affect the position of the laser.

The deflection does not affect the positional accuracy. However, the laser used to measure the frequency has some requirements that must be met. The laser has a measurement range of $0.3mm$. With a maximum deflection of less than $10\mu m$, the deflection will not overshoot the measurement range of the laser.

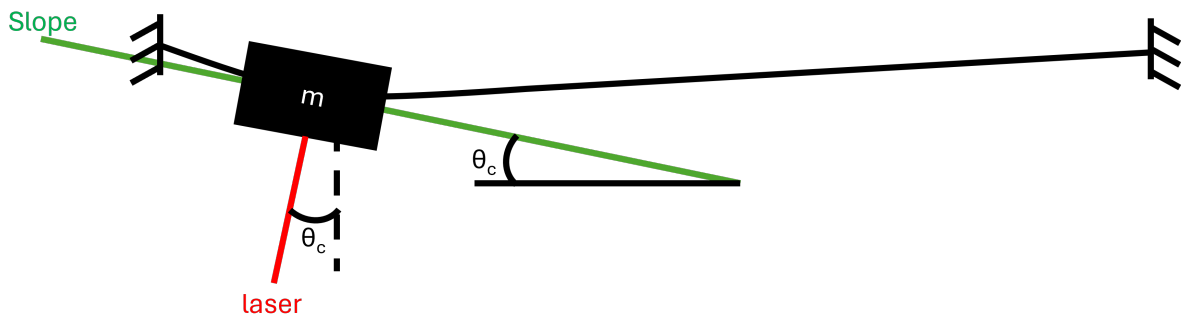


Figure 3.12: Angle by which the laser will deviate due to the deflection.

In summary, the axes exhibit a minor degree of deflection; however, this does not have a significant impact on positional or measurement accuracy. The deflection remains within a predictable range and does not induce substantial angular deviations that could potentially misalign the laser. Given that the maximum deflection is below the allowed positional tolerance of the system, any resultant displacement is negligible. A critical consideration is that, even if a minor angular deviation were to occur, its effect on positional accuracy would be minimal, especially over short distances. Thus, while the existence of deflection is recognised, it does not undermine the reliability of the measurement system. The axes sustain stability, guaranteeing that the laser positioning remains precise and adheres to the required accuracy standards.

3.2.2. Calibrating

Calibration is an essential procedure to ensure the accuracy and reliability of the system. In the absence of proper calibration, the measurements can become inconsistent, resulting in errors that affect the results. Consequently, this section delves into the calibration process for the testing setup.

Process

For the attainment of precise and reliable measurements, it is imperative to perform a system calibration. This procedure entails the adjustment and verification of the laser's alignment relative to the boundary of the oscillator. Initially, the system directs the laser to a specified location, as shown by the red circle in Figure 3.13. Subsequently, the laser advances incrementally toward the perimeter of the oscillator. Upon reaching the boundary, the system ceases movement, as illustrated in Figure 3.14, ensuring that the laser is accurately aligned with the oscillator's edge.

Laser

Flexous employs the Micro-Epsilon confocal IFS2405 laser for manual measurement of frequency. Given that this laser is used for determining the frequency of the oscillator, its incorporation into the design of the testing setup is advisable. Consequently, the laser must possess the capability to measure the oscillator's depth. Notably, the current methodology for frequency measurement involves assessing the time intervals when the laser is on the oscillator or off the oscillator. Therefore, this calibration approach is unlikely to encounter any issues.

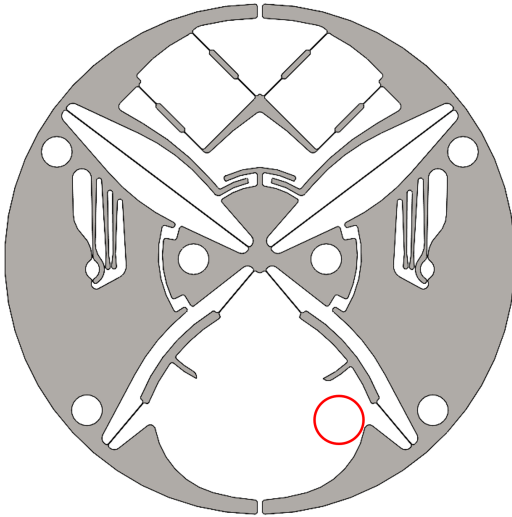


Figure 3.13: Position for laser placement to initiate calibration.

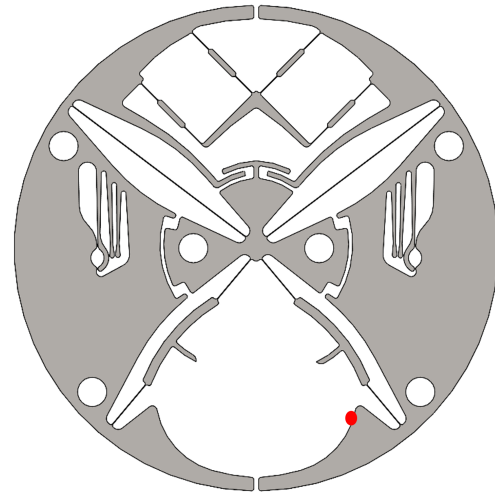


Figure 3.14: Laser aligned with the edge of the oscillator

3.2.3. Activation of vibration

Prior to measuring the frequency, it is imperative that the oscillator begin to vibrate. This initiation procedure guarantees that the oscillator attains a steady-state motion, thereby facilitating precise frequency detection. This section examines the methodology necessary for activation.

Design

The configuration of the activation mechanism is presented in Figure 3.15. It encompasses a speaker that produces an auditory signal. The sound waves emitted from one side of the speaker are captured within a narrow tube and subsequently channelled through a constricted aperture. As a result of being pressurised through this small opening, an airflow is generated, which is then directed through a tube towards the oscillator. Upon receiving an impulse from this airflow, the oscillator initiates vibration.

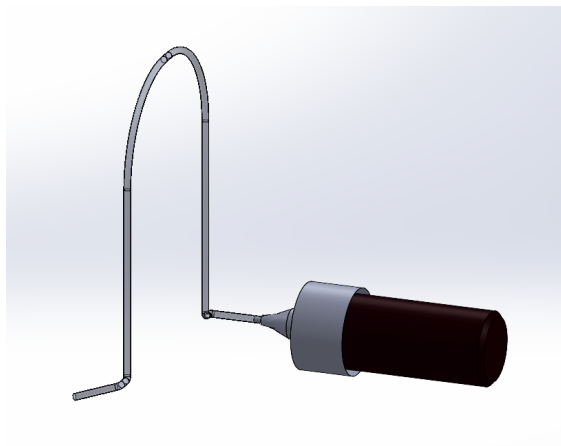


Figure 3.15: The activation system to activate the vibration of the oscillator

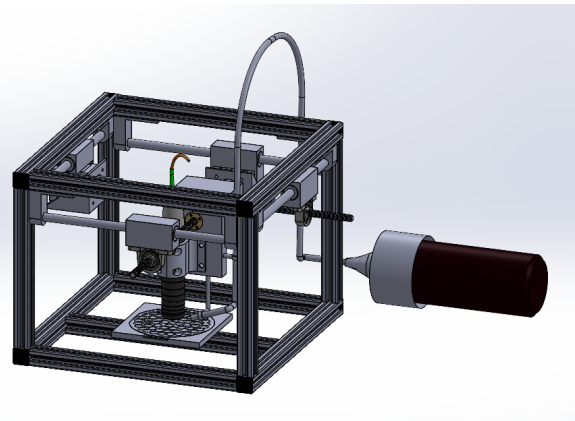


Figure 3.16: Complete overview of the design

3.2.4. Complete Design

Following the elucidation of all submechanisms, the entire design is delineated in Figure 3.16. This figure offers a perspective on the interaction and functionality of the various components. Each submechanism is instrumental in ensuring that the overall system runs with efficiency and reliability. The integration of these submechanisms has been engineered to optimise performance while preserving

structural integrity. The mechanical framework supports the various modules, ensuring that they function as intended without disruption. A fundamental attribute of the design is its modularity; Each sub-mechanism was developed independently prior to integration into the comprehensive system. This modular framework not only streamlines testing and debugging, but also accommodates future upgrades and modifications with minimal disturbance. In general, the combination of these submechanisms culminates in a robust and functional system poised for deployment in measuring the frequencies of the oscillators.

4

Testing & Results

4.1. Testing

This section delineates the testing plan and presents the associated results. Initially, it explicates the approach undertaken to formulate and execute the tests, encompassing the methodologies, criteria, and tools utilised. Subsequently, the results are systematically articulated, providing insight into the performance, effectiveness, and reliability of the evaluated components.

4.1.1. Changes

Flexous would like to see a proof of concept before investing in the setup. The configuration of Section 3.2.4 is similar to that of a 3D printer. That is why the Prusa I3 MK3 3D printer is used during the testing phase. There are some differences with respect to the design and the 3D printer. However, the main difference is that the printer uses timing belts to move the X and Y axes, which will be less accurate than the lead screws. Due to this change, not all the requirements from Section 2.4 are relevant anymore. The relevant requirements, especially the must haves, that are still valid are listed below.

Must Haves

1. The setup must be able to measure the frequency of 55 oscillators in one wafer in one running cycle.
2. The actuators must be able to position the oscillators with an accuracy of 10 microns.
3. The setup must have a control system that controls the adjustments of the axes.
4. The system must include an automatic calibration feature to maintain the accuracy of the measurements over time.

4.1.2. Setup

This section provides a detailed explanation of the measurement setups. In Figure 4.1, the arrangement for measuring the positions of the X and Y axes is illustrated. The movement of these axes is controlled by the code referenced in Appendix B.1. As depicted in Figure 4.1 (a), the laser aligns with the clamp of the confocal laser, facilitating displacement measurement as the X-axis moves. Moreover, as shown in Figure 4.1 (b), the laser concentrates on an additional block mounted on the 3D printer's bed, enabling the measurement of displacement when the Y-axis is in motion.

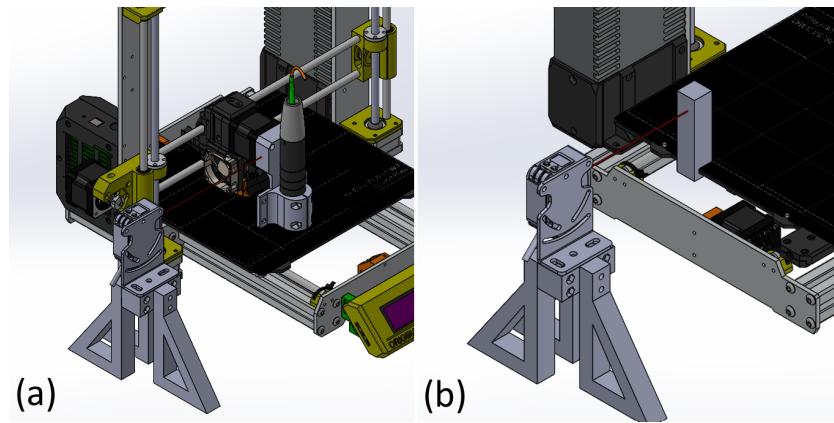


Figure 4.1: Setup for measuring the position. (a) setup for measuring the X axis. (b) setup for measuring the Y axis.

Figure 4.2 illustrates the setup to assess the calibration procedure. Figure 4.2 (a) depicts the laser employed for displacement measurement, which is focused on a small block connected to the thin object, whereas Figure 4.2 (b) indicates that the thin object incrementally advances towards the confocal laser. The code pertinent to the calibration process is available in Appendix B.2. This code executes a comparison between the current measurement and the previous measurement from the confocal laser. If the difference between these measurements exceeds a predefined threshold, the movement ceases. In contrast, if the difference is below the threshold, it invokes the `move_one_step` function of the moving code.

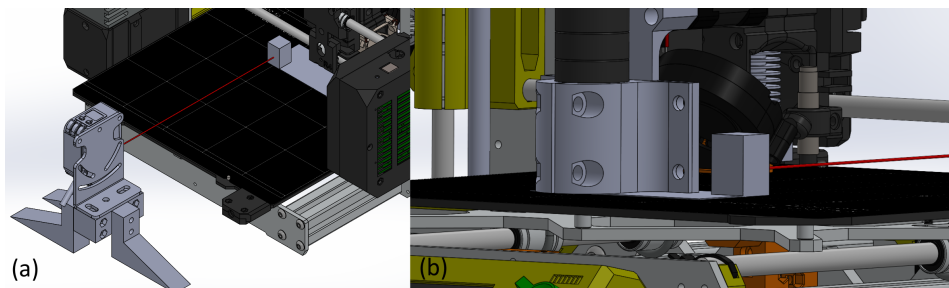


Figure 4.2: Setup for testing the calibration process for measurement. (a) the alignment of the laser to measure the displacement. (b) Y-axis moves slowly towards the confocal laser.

4.1.3. Plan

Test cases

This section delineates a comprehensive framework for the test cases to be conducted to ascertain the functionality, performance, and reliability of the system. The test cases address multiple facets of the system, incorporating both functional and non-functional testing. Functional test cases focus on verifying the core features and ensuring that each function performs accurately in alignment with the specified requirements. Non-functional test cases assess aspects such as performance to guarantee an optimal user experience. Each test case is detailed with explicit execution steps.

Table 4.1 details the experimental procedures employed to evaluate the accuracy and precision of the position. The initial column presents the test ID, serving as a reference point for each test. The subsequent 'Objective' column delineates the purpose of the test. In order to succeed in this, the steps and equipment columns detail the procedures undertaken and the apparatus employed in the execution of the test, respectively. The metrics column explicates the method by which the results are encapsulated. Table 4.2 illustrates the tests related to the calibration process.

Test ID	Objective	Steps	Equipment	Metrics
TP-001	Verify initial position (homing)	<ol style="list-style-type: none"> 1. Initiate the measurement at the zero reference point. 2. Set the measuring equipment to zero. 3. Relocate to an arbitrary position before executing the homing directive. 4. Read the position of the measuring equipment. 5. Repeat steps 3 and 4 a total of fifty times. 	Laser	The variability of the position in its home position.
TP-002	Test x-movement accuracy	<ol style="list-style-type: none"> 1. Initiate the measurement at the zero reference point. 2. Reposition the x-axis to a predetermined location. 3. Read the position of the measuring equipment. 4. Iterate over steps 2 and 3 for a total of five repetitions. 5. Repeat steps 2, 3, and 4 a total of ten times, altering the specified position following every fifth repetition 	Laser	The mean absolute error of the measured positions.
TP-003	Test y-movement accuracy	<ol style="list-style-type: none"> 1. Initiate the measurement at the zero reference point. 2. Reposition the y-axis to a predetermined location. 3. Read the position of the measuring equipment. 4. Iterate over steps 2 and 3 for a total of five repetitions. 5. Repeat steps 2, 3, and 4 a total of ten times, altering the specified position following every fifth repetition. 	Laser and block to measure the movement of the y-axis	The mean absolute error of the measured positions
TP-004	Test repeatability x-axis	<ol style="list-style-type: none"> 1. Initiate the measurement at the zero reference point. 2. Reposition the x-axis to a predetermined location. 3. Read the position of the measuring equipment. 4. Repeat steps 2, and 3 a total of fifty times. 	Laser	The mean and standard deviation of the measured positions.
TP-005	Test repeatability y-axis	<ol style="list-style-type: none"> 1. Initiate the measurement at the zero reference point. 2. Reposition the y-axis to a predetermined location. 3. Read the position of the measuring equipment. 4. Repeat steps 2, and 3 a total of fifty times. 	Laser and block to measure the movement of the y-axis	The mean and standard deviation of the measured positions.

Table 4.1: Test cases for testing the positional accuracy

Test ID	Objective	Steps	Equipment	Metrics
TC-001	Edge detection accuracy	<ol style="list-style-type: none"> 1. Put a thin object on the bed. 2. Slowly move the laser towards the object. 3. Measure the offset between the edge and the position where the laser stops moving. 4. Repeat these steps a total of fifty times. 	Laser	Precision of edge detection
TC-002	Speed variation	<ol style="list-style-type: none"> 1. Put a thin object on the bed. 2. Slowly move the laser towards the object. 3. Measure the offset between the edge and the position where the laser stops moving. 4. Iterate over steps 2 and 3 for a total of ten repetitions. 5. Repeat steps 2, 3, and 4 a total of 5 times, altering the speed following every tenth repetition 	Laser and thin object with a block to measure the movement of the y-axis	Correlation between the speed and stopping position.

Table 4.2: Test cases for testing the calibration process

4.2. Results

In this section, the results of the tests are presented and analysed. The data collected during the experiments are summarised in figures to highlight key trends and findings.

4.2.1. Verify Initial Position

The primary objective of test TP-001 is to evaluate the accuracy of the homing process within the 3D printer. Consistent variations in the home position can significantly affect the measurements. The results of this experiment are documented in Figure 4.3. The depicted plot is a box plot that contrasts the positional deviations along the X-axis and Y-axis of the 3D printer. The Y-axis quantifies the deviation in millimetres from the anticipated home position. According to the legend, the blue box indicates the deviations on the X-axis, whereas the orange box denotes those on the Y-axis. The box plots provide a visual representation of the deviations' distribution, encompassing the interquartile range (IQR), median, mean (denoted by the 'X' marker), and outliers.

The deviations along the X-axis exhibit a broader interquartile range compared to the Y-axis, indicating increased variability in positioning precision along this direction. Conversely, the Y-axis deviations demonstrate a more confined distribution, implying enhanced repeatability and consistency in homing along this axis. The median values on both axes reflect minor deviations from the anticipated homing position, which is preferable for precision control. However, the X-axis displays several outliers, with deviations extending beyond 0.05 mm, denoting instances where the homing position significantly deviated beyond the expected range.

The findings suggest that the homing procedure demonstrates a high degree of precision, characterised by deviations within the micrometre scale. The variability along the X-axis is comparatively greater than along the Y-axis, and the existence of outliers is less ideal. However, these results indicate that the positioning of the laser is unlikely to be substantially affected by the homing process.

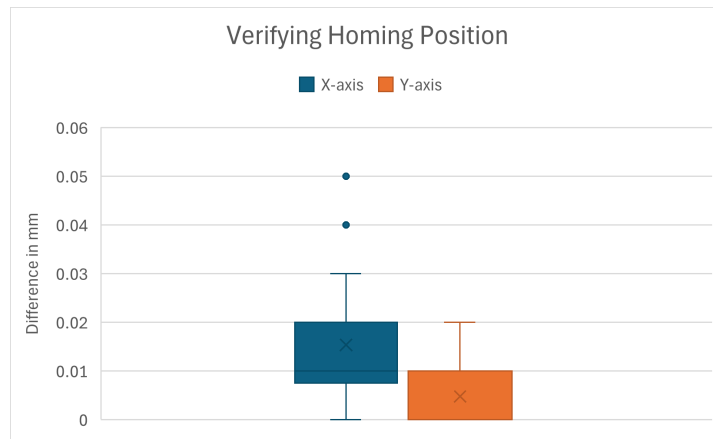


Figure 4.3: Whisker diagrams of the difference between begin and end position of the home position

4.2.2. Accuracy of X and Y axis

Tests TP-002 and TP-003 are dedicated to assessing the precision of the axes. Due to the diminutive size of the oscillators, there is limited space available for optimal laser positioning. Consequently, one of the stipulated requirements is that the system must achieve a positional accuracy of 10 microns. The results of these experiments are depicted in Figure 4.4 and Figure 4.5. These figures present the mean absolute error (MAE) on both the X-axis and the Y-axis. The scatter plots offer information about the accuracy of the measurement system at various distances. The errors, quantified in millimetres, underscore potential inconsistencies or systematic biases in the system's performance.

Figure 4.4 delineates the correlation between distance and the mean absolute error along the X-axis. The data show variability across varying distances, with certain points exhibiting relatively minor errors (below 0.1 mm), while others attain approximately 0.2 mm. Notably, there are undulating fluctuations in error magnitude, lacking a discernible trend of escalation or decline. In parallel, Figure 4.5 elucidates the mean absolute error on the Y-axis as it corresponds to distance. In comparison to the X-axis errors, the errors along the Y-axis are observed to be greater, with some values approaching 0.5 mm. The dispersion of errors implies a variability contingent upon distances, with certain distances producing markedly higher errors than others.

The errors observed along the Y-axis exhibit greater magnitude than those on the X-axis, potentially indicating a systematic issue within the experimental setup. The occurrence of larger outliers in the error distribution along the Y-axis suggests that accuracy may be substantially compromised at certain distances. These errors could be attributable to limitations in the resolution of the laser sensor used in the experiment, as the precision of the sensors can inherently introduce errors [13]. Additionally, considering that the accuracy of a 3D printer ranges between 0.1 and 0.2 mm, these findings are largely anticipated, notwithstanding the presence of some outliers.

The findings of this experiment demonstrate that the measurement system shows increased variability in error along the Y-axis relative to the X-axis. The absence of a definitive correlation between distance and error implies that both systematic and random factors play a role in the observed inaccuracies.

4.2.3. Repeatability of X and Y axis

The investigations designated as TP-004 and TP-005 aim to assess repeatability along the X-axis and the Y-axis. Repeatability is indicative of the system's capability to consistently relocate to the same reference point. The results of these experiments are documented in Figure 4.6 and Figure 4.7. These figures elucidate the findings of a repeatability analysis performed on the X-axis and Y-axis, employing statistical evaluations rooted in normal distribution. The primary aim of this experiment is to study the deviation of measured distances from a predefined target value, as well as to determine both the accuracy and precision of the system. The two graphs illustrate the probability density functions of the measurements obtained along the X and Y axes, juxtaposed with their respective target values.

Figure 4.6 presents the normal distribution of the measured distances along the X-axis. The X-axis of the graph represents the measured distance in millimetres. The plotted normal distribution curve (in blue) indicates the spread of the measurements. Additionally, the target value (in orange) is placed

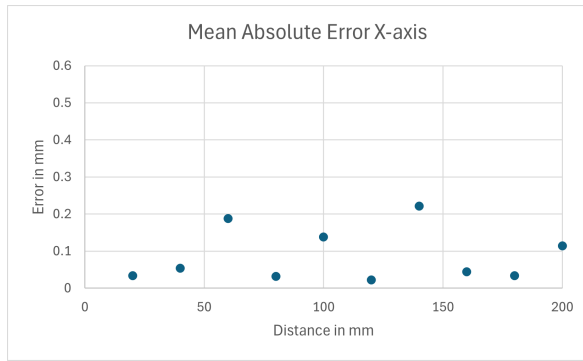


Figure 4.4: Accuracy of the X-axis

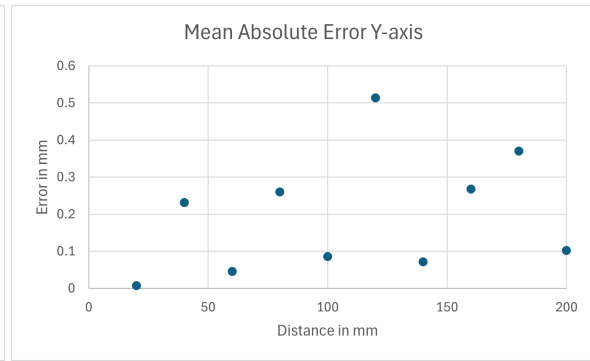


Figure 4.5: Accuracy of the Y-axis

at 100 mm, while the mean of the measured values (in green) is located at approximately 100.15 mm. Figure 4.7 displays similar data for the Y-axis. Here, the normal distribution is centred around a mean value of approximately 99.85 mm, while the target value is 100 mm. This suggests a negative deviation in the Y-direction.

As elucidated in Figure 2.1, repeatability is characterized by the width of the normal distribution, whereas accuracy is defined as the distance between the target value and the mean. The normal distribution of the Y-axis exhibits a slightly narrower width compared to that of the X-axis, suggesting marginally superior repeatability along the Y-axis. References Figure 4.6 and Figure 4.7 report an accuracy of approximately 0.15 mm. When this value is juxtaposed with the error associated with a distance of 100 mm, as documented in Figure 4.4 and Figure 4.5, it is found to be comparable.

The analysis of repeatability on the X and Y axes using normal distribution statistics reveals that the system exhibits systematic bias but good precision. The mean values consistently deviate from the target in both axes. However, the narrow distribution suggests high repeatability, which means that, although the system is not perfectly accurate, it is consistent in its positioning.

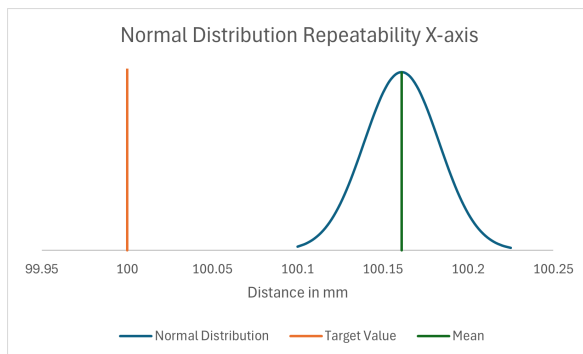


Figure 4.6: Normal distribution of the repeatability of the X-axis

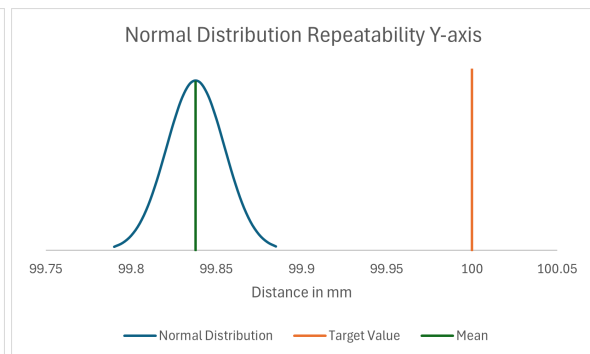


Figure 4.7: Normal distribution of the repeatability of the Y-axis

4.2.4. Edge Detection Accuracy

This experiment focusses on the alignment of the laser with the edge of the oscillator. Ensuring precise alignment is crucial for reliable frequency measurements. If the laser is misaligned, even slightly, the data integrity is compromised, leading to inaccuracies in the results. Therefore, it is critical that the calibration procedure halts immediately once the laser reaches the edge of the oscillator. The outcome of this meticulous alignment process is depicted in detail in Figure 4.8.

The figure illustrates a normal distribution pertaining to the edge detection process, where the X-axis denotes the discrepancy between the edge and the laser in millimeters. The experimental mean is approximately 0.6 mm, indicating that, on average, the calibration process halts 0.6 mm later than intended. The associated code for the calibration procedure is specified in Appendix B.2. Conversely, Flexous has implemented code that inputs laser data into a buffer, executing every 10 milliseconds.

The printer operates at a predefined speed; thus, investigating the influence of speed on the precision of edge detection is warranted and will be the focus of the subsequent experiment.

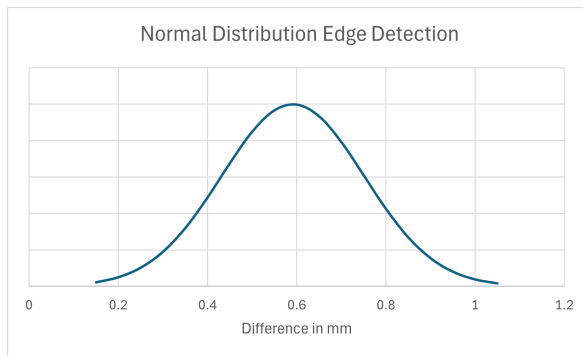


Figure 4.8: Normal distribution of the difference from the edge detection test.

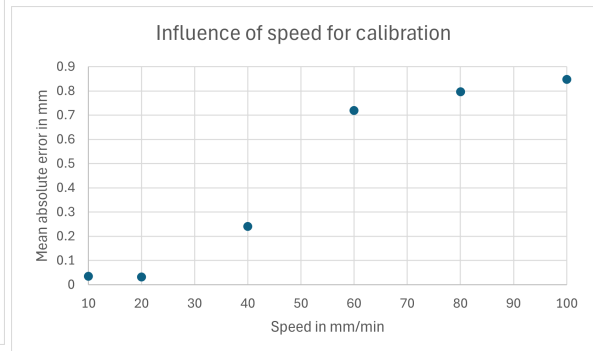


Figure 4.9: Influence of speed on the edge detection

4.2.5. Edge Detection Speed

The prior test was conducted at a velocity of 100, which proved to be excessively rapid. Consequently, the objective of this experiment is to determine the optimal velocity that facilitates the precise alignment of the laser with the edge of the oscillator. The findings of this experiment are detailed in Figure 4.9.

The figure illustrates the relationship between the speed in millimetres per minute on the x-axis and the mean absolute error, quantified in millimetres on the y-axis. The graph displays six data points, each corresponding to the mean absolute error recorded at different calibration speeds: 10, 20, 40, 60, 80, and 100 mm/min. The data indicate an observable positive correlation between the calibration speed and the magnitude of the error, suggesting that the calibration speed increases.

Within the lower end of the velocity spectrum, specifically at 10 and 20 mm/min, the mean absolute error remains minimal, marginally exceeding 0.03 mm. These measurements denote a substantial degree of precision and accuracy at reduced movement speeds. The extremely low error rates at these velocities imply that the system has sufficient time to accurately capture positional data or implement adjustments, which yields highly reliable results. At a moderate speed of 40 mm/min, there is a discernible increase in the mean absolute error. This increase signifies a considerable deviation from the error observed at 20 mm/min, indicating the initiation of limitations within the calibration process attributable to speed-related factors. At this velocity, the latency between the incoming data and the printer response becomes apparent. From 60 mm/min onwards, the increase in mean absolute error becomes even more significant.

The results of this experiment unequivocally demonstrate that the accuracy of calibration is intricately linked to the operational velocity. While lower speeds yield exceptionally low mean absolute errors, signifying precise calibration, elevated speeds engender considerable errors that compromise the efficacy of the calibration procedure.

4.3. Overall result

The positional accuracy observed in the TP-002 and TP-003 assessments did not meet the desired standards. These evaluations demonstrated that positional accuracy was insufficient for the specified requirements. However, when applying this level of positional accuracy to navigate to the region highlighted in Figure 3.13 and conducting the calibration procedure, the system exhibits an error margin of approximately 0.03 mm. Consequently, the positional accuracy of the system is determined to be 0.03 mm.

5

Discussion & Conclusion

This study focused on evaluating the positional accuracy, repeatability, and calibration efficacy of a laser-assisted measurement system integrated with a Prusa I3 MK3 3D printer. The testing phase, which included homing procedures, movement trials, and edge detection experiments, revealed both the system's capabilities and its limitations, providing valuable insight for precision-based applications.

5.1. Homing accuracy

The homing tests demonstrated substantial positional consistency, particularly along the Y-axis, which outperformed the X-axis with a smaller interquartile range and fewer outliers. These results confirm the reliability of the homing process, a critical factor in automated measurement systems that rely on precise and repeatable initialization. However, the variability observed on the X-axis points to mechanical or firmware-related inconsistencies that merit further investigation. Improving endstop accuracy or refining firmware routines could reduce the occurrence of outliers and narrow the deviation range.

5.2. Movement Accuracy

The movement accuracy tests were designed to evaluate the precision with which the system could reach a specified position from a predetermined reference point. The Mean Absolute Error (MAE) analysis over different distances demonstrated that the Y-axis persistently exhibited a higher error compared to the X-axis. Although this could be partially attributed to sensor alignment or mechanical characteristics of the movement system, it should be noted that the measurement block employed for the Y-axis test might have also contributed to increased uncertainty.

In particular, the absence of a direct correlation between travel distance and absolute error suggests that the inaccuracies may not be solely systematic. Rather, a combination of random error sources, such as stepper motor microstepping inconsistencies, belt elasticity, or thermal expansion, along with minor misalignments, are likely contributing factors. Despite these limitations, most of the measured deviations remained below 0.1 mm.

5.3. Repeatability

The capability of the system to revert to an identical position following multiple movements is essential to maintain consistent results. Both axes exhibited significant repeatability in these evaluations, with the Y-axis once again demonstrating superior performance, as evidenced by a narrower distribution and reduced scatter in the normal curve plot. Despite a persistent offset between the actual returned position and the intended target (approximately 0.15 mm in both axes), the tight clustering of repeated measurements suggests that the system error is predominantly systematic rather than random.

Such systematic biases are frequently observed in open-loop systems, similar to those used in 3D printers, where the accuracy of movements is presumed unless explicitly rectified. The predictable nature of this deviation offers an opportunity for rectification through hardware-based compensation. By incorporating a closed-loop feedback mechanism, it would be feasible to identify and actively rectify any positional discrepancies as they arise.

5.4. Calibration & Edge Detection

The findings of TC-001 demonstrated a distinct and consistent offset between the detected edge and the actual edge, with an average deviation of approximately 0.6 mm. This discrepancy was mainly attributed to the default speed settings in the calibration script, which had not been optimised for precise halting at the edge. To further explore this issue, the subsequent test (TC-002) evaluated the impact of varying the calibration speeds on the detection accuracy. As hypothesised, lower speeds resulted in markedly reduced errors, with measurements at 10 and 20 mm/min producing mean absolute errors of less than 0.05 mm. In contrast, as the speeds increased, the positional error also increased, with values increasing significantly above 40 mm/min. These results suggest a direct trade-off between operational speed and edge detection fidelity.

The observed error is attributable to a combination of physical factors, including the momentum of the system and the finite update rate of the sensor, as well as software constraints, such as the rate at which sensor readings are analysed and acted upon. At elevated velocities, the system's inability to decelerate promptly upon edge detection results in overshoot.

5.5. Future Work

While the current study has provided valuable insights, several avenues remain open for further exploration. Future work will aim to build on the findings presented here, address current limitations, and expand the scope to improve the accuracy and broader applicability of the system.

Prospective research could explore the implementation of real-time feedback correction or closed-loop control systems, wherein positional data obtained from external sensors may be employed to dynamically modulate the final positioning of the toolhead. Such systems could significantly improve the accuracy and repeatability of the current setup by continuously monitoring deviations and correcting them in real time. Integrating high-resolution encoders or vision-based tracking systems could further improve spatial accuracy.

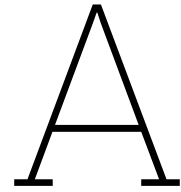
Predictive stopping logic is a system enhancement that leverages real-time data to improve efficiency. By analysing velocity, deceleration, and other relevant parameters, the system can predict the optimal stopping point with more accuracy. This reduces reaction times and minimises errors. The anticipation of the detection point allows for smooth transitions and proactive adjustments, enhancing overall system performance. Implementing this approach could lead to significant advancements in operational efficiency.

Adjusting the printer's firmware to support finer motor control could reduce deviations during both homing and movement. Enhancing the resolution of microstepping or optimising motion algorithms would allow for smoother and more precise movements. Improved homing procedures, including slower approach speeds and repeat homing sequences, could also reduce the variability in toolhead positioning.

In conclusion, a high-precision measurement system for Flexous oscillators can be effectively developed by combining a mechanically stable platform, such as a modified 3D printer, with an integrated laser and edge detection module. Precision is achieved through calibration, meaning low-speed movement until the laser detects the edge. Optimisation can be pursued by implementing closed-loop control systems, refining firmware for accurate homing and positioning, and employing predictive algorithms that account for motion dynamics. Through these strategies, the system can reliably align with oscillator structures and enable accurate frequency measurements directly on the wafer, eliminating the need for manual intervention.

References

- [1] C. Landesberger, S. Scherbaum, and K. Bock, "Carrier techniques for thin wafer processing," May 17, 2007.
- [2] D. Collins. "What's the difference between minimum incremental motion and resolution," Linear Motion Tips. (Dec. 24, 2020), [Online]. Available: <https://www.linearmotiontips.com/difference-between-minimum-incremental-motion-and-resolution/> (visited on 01/28/2025).
- [3] TQP. "Accuracy and precision | what is precision in measurement?" Tech Quality Pedia. (Mar. 17, 2021), [Online]. Available: <https://techqualitypedia.com/accuracy-and-precision/> (visited on 02/20/2025).
- [4] "MoSCoW prioritization," ProductPlan. (), [Online]. Available: <https://www.productplan.com/glossary/moscow-prioritization/> (visited on 08/13/2024).
- [5] A. Arnau Vives, Ed., *Piezoelectric Transducers and Applications*, Berlin, Heidelberg: Springer, 2004, ISBN: 978-3-662-05363-8 978-3-662-05361-4. DOI: 10.1007/978-3-662-05361-4. (visited on 04/09/2025).
- [6] S. Wang, W. Rong, L. Wang, H. Xie, L. Sun, and J. K. Mills, "A survey of piezoelectric actuators with long working stroke in recent years: Classifications, principles, connections and distinctions," *Mechanical Systems and Signal Processing*, vol. 123, pp. 591–605, May 15, 2019, ISSN: 0888-3270. DOI: 10.1016/j.ymsp.2019.01.033.
- [7] "The ultimate guide to selection piezo products," Xeryon. (), [Online]. Available: <https://xeryon.com/piezo-selection-guide/> (visited on 01/02/2025).
- [8] A. V. S. Otoni, J. J. P. Z. de Souza Tavares, and R. M. F. Neto, "3d printer as a resource for didactic development tool for the maker culture—an open-source design of the COREXY 3d printer," in *Perspectives and Trends in Education and Technology*, ISSN: 2190-3026, Springer, Singapore, 2023, pp. 175–185, ISBN: 978-981-9954-14-8. DOI: 10.1007/978-981-99-5414-8_18.
- [9] "Microstepping," Dover Motion. (), [Online]. Available: <https://dovermotion.com/resources/motion-control-handbook/microstepping/> (visited on 01/28/2025).
- [10] D. Florian. "How to build a 3d printer: Microstepping." (), [Online]. Available: <https://www.drdflo.com/pages/Guides/How-to-Build-a-3D-Printer/Microstepping.html> (visited on 01/28/2025).
- [11] "Leadscrew moer, anti-backlash, TR8x2 123-3d 123-3d.nl." (), [Online]. Available: https://www.123-3d.nl/123-3D-Leadscrew-moer-anti-backlash-TR8x2-i2213-t9712.html?gad_source=1&gclid=CjwKCAiAiaC-BhBEEiwAjY99qFrqKR8q-alySrjz5YtcJXgQXOmWDQ1BN92VyNR5WG5criPbzGkyGRoCtxYQAvD_BwE (visited on 03/05/2025).
- [12] O. Vahid Araghi, "Friction-induced vibration in lead screw systems," Ph.D. dissertation, University of Waterloo, 2009-05-13.
- [13] G. Häusler and S. Ettl, "Limitations of optical 3d sensors," in *Optical Measurement of Surface Topography*, Springer, Berlin, Heidelberg, 2011, pp. 23–48, ISBN: 978-3-642-12012-1. DOI: 10.1007/978-3-642-12012-1_3.



Deflection Calculation

This appendix will show the calculation for the deflection of the guiding rails.

Free Body Diagram

The free body diagram, shown in Figure A.1, is a simple, visual representation of the guiding rails and all the external forces that act on it.

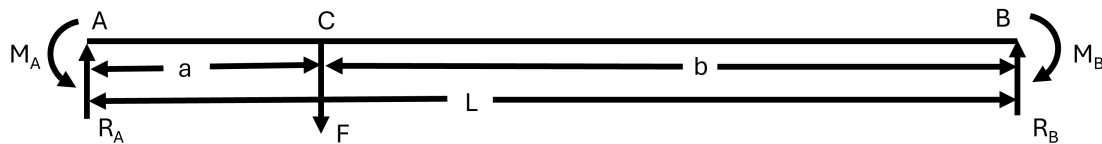


Figure A.1: Free Body Diagram of the situation

Moment Diagram

To calculate the reaction forces (R_A , R_B , M_A and M_B), the free moment and fixed moment diagrams should be drawn. To draw the Free Moment Diagram, consider the beam simply supported as shown in Figure A.2. From this simply supported beam, the moment in point C can be calculated.

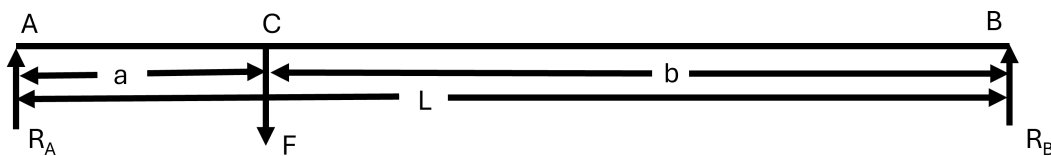


Figure A.2: Beam simply supported by R_A and R_B

$$\begin{aligned}
 + \circlearrowleft \sum M = 0 &\Rightarrow R_B L - F a = 0 \Rightarrow R_B = \frac{F a}{L} \\
 + \uparrow \sum F = 0 &\Rightarrow R_A + R_B - F = 0 \Rightarrow R_A = F - \frac{F a}{L} = \frac{F(L - a)}{L} = \frac{F b}{L} \\
 M_C = R_A a &= \frac{F a b}{L}
 \end{aligned}
 \tag{A.1}$$

The Fixed Moment Diagram can be drawn considering that M_A is bigger than M_B , because the force is closer to point A than to point B. The Free Moment Diagram and Fixed Moment Diagram are shown in Figure A.3.

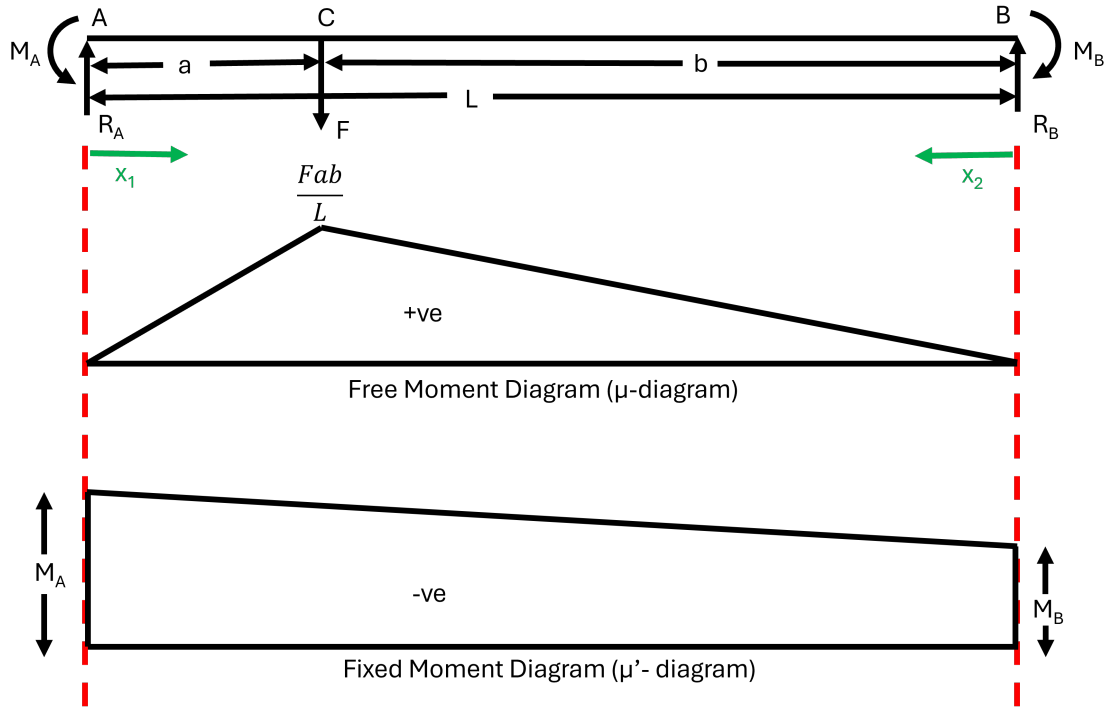


Figure A.3: Diagrams of the Free and Fixed moment

Reaction Forces

The reaction force can now be calculated because the area of μ -diagram should be equal to the area of μ' -diagram. In addition, the centroidal distances of both diagrams should be equal to each other.

$$\begin{aligned} \text{area } \mu\text{-diagram} &= \frac{1}{2}L \frac{Fab}{L} = \frac{Fab}{2} \\ \text{area } \mu'\text{-diagram} &= M_B L + \frac{1}{2}L(M_A - M_B) = \frac{L(M_A + M_B)}{2} \end{aligned} \quad (\text{A.2})$$

$$\frac{Fab}{2} = \frac{L(M_A + M_B)}{2} \Rightarrow M_A + M_B = \frac{Fab}{L}$$

β is the centroidal distance of μ -diagram from the left and γ is the centroidal distance of μ' -diagram from the left.

$$\begin{aligned} \beta &= \frac{L+a}{3} \\ \gamma &= \frac{L}{3} \left(\frac{M_A + 2M_B}{M_A + M_B} \right) \end{aligned} \quad (\text{A.3})$$

$$\frac{L+a}{3} = \frac{L}{3} \left(\frac{M_A + 2M_B}{M_A + M_B} \right) \Rightarrow M_A + 2M_B = \frac{Fab}{L^2}(L+a)$$

Subtract the result from Equation (A.2) from the result of Equation (A.3) gives:

$$\begin{aligned} M_A + 2M_B - M_A - M_B &= \frac{Fab}{L^2}(L+a) - \frac{Fab}{L} \\ M_B &= \frac{Fab}{L} + \frac{Fa^2b}{L^2} - \frac{Fab}{L} = \frac{Fa^2b}{L^2} \\ M_A &= \frac{Fab}{L} - M_B = \frac{Fab^2}{L^2} \end{aligned} \quad (\text{A.4})$$

To calculate R_A and R_B , the sum of the moments and the sum of the forces should be equal to 0.

$$\begin{aligned}
 + \circlearrowleft \sum M_B = 0 &\Rightarrow \frac{Fa^2b}{L^2} - Fb + R_AL - \frac{Fab^2}{L^2} = 0 \\
 R_AL &= Fb + \frac{Fab^2}{L^2} - \frac{Fa^2b}{L^2} = Fb \left(\frac{L^2 + ab - a^2}{L^2} \right)
 \end{aligned} \tag{A.5}$$

$$R_A = \frac{Fb}{L^3}(L^2 + ab - a^2) = \frac{Fb^2}{L^2}(3a + b)$$

$$\begin{aligned}
 + \uparrow \sum F_y = 0 &\Rightarrow R_A + R_B - F = 0 \\
 R_B = F - R_A &= F - \frac{Fb^2}{L^2}(3a + b) = \frac{Fa^2}{L^3}(a + 3b)
 \end{aligned} \tag{A.6}$$

The reaction forces are $R_A = \frac{Fb^2}{L^2}(3a + b)$, $R_B = \frac{Fa^2}{L^3}(a + 3b)$, $M_A = \frac{Fab^2}{L^2}$, and $M_B = \frac{Fa^2b}{L^2}$.

Deflection

The deflection, y , can be calculated by integrating the moment twice. With the first integration, the formula for the angular displacement, θ , will be calculated. The formulas for the deflection and angular displacement between points A and C will be computed the following way.

$$\begin{aligned}
 + \circlearrowleft \sum M_{x_1} = 0 &\Rightarrow M_{x_1} = -\frac{Fab^2}{L^2} + \frac{Fb^2(3a + b)}{L^3}x_1 \\
 EI \frac{d^2 y_{AC}}{dx_1^2} &= M_{x_1} = -\frac{Fab^2}{L^2} + \frac{Fb^2(3a + b)}{L^3}x_1 \\
 EI \frac{dy_{AC}}{dx_1} &= -\frac{Fab^2}{L^2}x_1 + \frac{Fb^2(3a + b)}{2L^3}x_1^2 + C_1 \\
 EI y_{AC} &= -\frac{Fab^2}{2L^2}x_1^2 + \frac{Fb^2(3a + b)}{6L^3}x_1^3 + C_1x_1 + C_2
 \end{aligned} \tag{A.7}$$

The angular displacement and the deflection are zero when x_1 is zero.

$$\begin{aligned}
 \theta = 0 \text{ at } x_1 = 0 &\Rightarrow C_1 = 0 \\
 y_{AC} = 0 \text{ at } x_1 = 0 &\Rightarrow C_2 = 0
 \end{aligned} \tag{A.8}$$

Therefore, the formulas for the angular displacement and the deflection between points A and C are:

$$\begin{aligned}
 y_{AC} &= -\frac{Fb^2x_1^2}{6EIL^3}(3aL - 3ax_1 - bx_1) \\
 \theta_{AC} &= -\frac{Fb^2x_1}{2EIL^3}(2aL - 3ax_1 - bx_1)
 \end{aligned} \tag{A.9}$$

The same method can be used to compute the formulas for the deflection and angular displacement between points C and B. However, for simplicity, the origin will now be on the right side, so x_2 can be used.

$$\begin{aligned}
 + \circlearrowleft \sum M_{x_2} = 0 &\Rightarrow M_{x_2} = -\frac{Fa^2b}{L^2} + \frac{Fa^2(a + 3b)}{L^3}x_2 \\
 EI \frac{d^2 y_{CB}}{dx_2^2} &= M_{x_2} = -\frac{Fa^2b}{L^2} + \frac{Fa^2(a + 3b)}{L^3}x_2 \\
 EI \frac{dy_{CB}}{dx_2} &= -\frac{Fa^2b}{L^2}x_2 + \frac{Fa^2(a + 3b)}{2L^3}x_2^2 + C_3 \\
 EI y_{CB} &= -\frac{Fa^2b}{2L^2}x_2^2 + \frac{Fa^2(a + 3b)}{6L^3}x_2^3 + C_3x_2 + C_4
 \end{aligned} \tag{A.10}$$

The angular displacement and the deflection are zero when x_2 is zero.

$$\begin{aligned}\theta &= 0 \text{ at } x_2 = 0 \Rightarrow C_3 = 0 \\ y_{CB} &= 0 \text{ at } x_2 = 0 \Rightarrow C_4 = 0\end{aligned}\tag{A.11}$$

Therefore, the formulas for the angular displacement and the deflection between points C and B are:

$$\begin{aligned}y_{CB} &= -\frac{Fa^2x_2^2}{6EIL^3}(3bL - 3bx_2 - ax_2) \\ \theta_{CB} &= -\frac{Fa^2x_2}{2EIL^3}(2bL - 3bx_2 - ax_2)\end{aligned}\tag{A.12}$$

These formulas can be rewritten with respect to x_1 , because $x_2 = L - x_1$.

$$\begin{aligned}y_{CB} &= -\frac{Fa^2(L-x_1)^2}{6EIL^3}(3bL - 3b(L-x_1) - a(L-x_1)) \\ &= -\frac{Fa^2(L-x_1)^2}{6EIL^3}(3bx_1 - aL + ax_1) \\ \theta_{CB} &= -\frac{Fa^2(L-x_1)}{2EIL^3}(2bL - 3b(L-x_1) - a(L-x_1)) \\ &= -\frac{Fa^2(L-x_1)}{2EIL^3}(x_1(3b+a) - L^2)\end{aligned}\tag{A.13}$$

Deflection at Point C

To obtain the angular displacement and deflection at point C, substitute x_1 for a because the distance between point A and C is a .

$$\begin{aligned}y_C &= -\frac{Fa^2b^2}{6EIL^3}(3aL - 3a^2 - ab) = -\frac{Fa^3b^3}{3EIL^3} \\ \theta_C &= -\frac{Fab^2}{2EIL^3}(2aL - 3a^2 - ab) = -\frac{Fa^2b^2}{2EIL^3}(b-a)\end{aligned}\tag{A.14}$$

B

Code

The code shared in this Appendix is only code that is made by the author. Flexous already has made a programme for measuring the frequency of the oscillator, but that piece of code cannot be shown. There will be some classes that Flexous had written itself used in the code share in this Appendix.

B.1. Code for Movement

```
1  import serial
2  import time
3
4  class MovingPrinter:
5      def __init__(self, bed_x=250, bed_y=210):
6          # Initialize serial connection to the 3D printer
7          self.serial_connection = serial.Serial("COM3", 115200, timeout=2) #
8          → Replace 'COM3' with your printer's serial port and adjust the
9          → baudrate as necessary
10         time.sleep(2) # Give some time for the connection to initialize
11
12         self.bed_x = bed_x
13         self.bed_y = bed_y
14
15     def gcode(self, command):
16         # Send a G-code command to the printer and wait for acknowledgment
17         command += "\n"
18         self.serial_connection.write(command.encode())
19         # print(f"Sending command: {command.strip()}") # Show the command for
20         → debugging
21
22     def send_command(self, command):
23         # Wait for the printer reached its position before sending a new command.
24         self.gcode(command)
25         self.check_moving()
26
27     def check_moving(self):
28         self.gcode("M400")
29
30     def home(self):
31         # Homing command to reset all axes to their origin
32         command = "G28 X Y"
33         return self.send_command(command)
```

```

32     def move_linear(self, x=None, y=None, z=None):
33         # Command for linear movement with optional x, y, and z parameters
34         command = "G1"
35
36         if x is not None:
37             command += f" X{x}"
38         if y is not None:
39             command += f" Y{y}"
40         if z is not None:
41             command += f" Z{z}"
42
43         self.send_command(command)
44
45     def move_one_step(self, axis='Y', distance=0.1):
46         # Make a small movement on the specified axis.
47
48         # Switch to relative positioning mode
49         self.gcode("G91")
50
51         # Move by a small distance
52         command = f"G1 {axis}{distance} F100" # F100 sets feed rate (speed)
53         self.send_command(command)
54
55         # Switch back to absolute positioning
56         self.gcode("G90")
57
58     def move_to_center(self):
59         self.move_linear(x=self.bed_x/2, y=self.bed_y/2)
60
61
62     def close(self):
63         # Close the serial connection
64         if self.serial_connection.is_open:
65             self.serial_connection.close()
66             print("Serial connection closed.")

```

B.2. Code for Calibration

```

1  class Calibration:
2      def __init__(self, printer, gui):
3          self.gui = gui
4          self.threshold = 0.00001
5
6          self.printer = printer
7
8      def compare_measurements(self, current_measurement, new_measurement):
9          return abs(new_measurement - current_measurement)
10
11     def run_calibration(self, dist):
12         #run calibration to ensure the measurement will be done on the right spot.
13         current_measurement = dist[-2]
14         new_measurement = dist[-1]
15
16         difference = self.compare_measurements(current_measurement,
17         ↪ new_measurement)

```

```
17     if difference > self.threshold:
18         print("Difference exceeds threshold. Stopping calibration.")
19         self.gui.close_window()
20     else:
21         self.printer.move_one_step()
```
